

RESEARCH ARTICLE

Effects of assimilation of YOPP-SH additional radiosonde observations on analyses and forecasts over Antarctica in austral summer

Yonghan Choi¹  | Seong-Joong Kim¹  | David H. Bromwich²  |
Jordan G. Powers³ | Hataek Kwon⁴ | Sang-Jong Park¹ 

¹Division of Atmospheric Sciences,
Korea Polar Research Institute, Incheon,
Republic of Korea

²Polar Meteorology Group, Byrd Polar and
Climate Research Center, The Ohio State
University, Columbus, Ohio, USA

³Mesoscale & Microscale Meteorology
Lab, National Center for Atmospheric
Research, Boulder, Colorado, USA

⁴School of Earth and Environmental
Sciences, Seoul National University,
Seoul, Republic of Korea

Correspondence

Sang-Jong Park, Division of Atmospheric
Sciences, Korea Polar Research Institute,
26 Songdomirae-ro, Yeonsu-gu, Incheon
21990, Republic of Korea.
Email: sangjong@kopri.re.kr

Funding information

Korea Polar Research Institute,
Grant/Award Number: PE23030; National
Research Foundation of Korea (NRF),
Grant/Award Number:
NRF-2023R1A2C1008238

Abstract

Radiosonde observations over Antarctica and the surrounding oceans were enhanced during the Year of Polar Prediction in the Southern Hemisphere (YOPP-SH) summer Special Observing Period (SOP). Observing System Experiments (OSEs) were conducted in a continuous cycling framework using the Weather Research and Forecasting (WRF) Model and its data assimilation system. Routinely available observations were assimilated in the CTL (control) experiment, and special radiosonde observations from the YOPP-SH SOP were additionally assimilated in the YOPP experiment. The results were compared to investigate the effects of additional radiosonde observations on analyses and forecasts over and around Antarctica. Verifications against ERA5 re-analysis, radiosonde observations, and Automatic Weather Station (AWS) observations show overall positive effects of additional radiosonde observations. These positive effects are most noticeable in temperature at lower levels at earlier forecast lead times; afterward, wind forecast improvements at upper levels are the most noticeable. Although routine and special radiosonde observations are concentrated over the eastern and coastal regions of Antarctica (compared to the western and inland regions), the effects of the extra data spread in longitudinal and latitudinal directions; therefore, the effects on the forecasts are not limited to only the areas near the radiosonde observations. A case study reveals how cyclone forecasts are improved through the assimilation of the additional YOPP-SH SOP radiosonde observations. This study provides insights into future observation strategies in Antarctica, such as horizontal/vertical observation locations, observation variables, and so forth to maximize effects of new observations on forecasts over Antarctica.

KEYWORDS

Data assimilation, radiosonde observations, verification, YOPP-SH SOP

1 | INTRODUCTION

There has been increasing interest in the polar regions in a changing climate because temperature increase and associated sea ice melting over the Arctic Ocean and glacial melting in West Antarctica are key factors driving extreme weather and climate events (e.g., Jun *et al.*, 2020; Cohen *et al.*, 2021). Accurate forecasts over polar regions are still challenging, however, because limitations in physics parameterizations and initial/boundary conditions over the high latitudes remain large. Errors in the initial conditions can be lessened through the use of improved data assimilation (DA) methods and/or more observations. Although radiance observations from polar-orbiting satellites can reduce errors in initial conditions, assimilating radiance observations over polar regions is significantly limited owing to surface properties (e.g., sea ice and snow) (Lawrence *et al.*, 2019). The density of conventional observations, such as radiosonde, is comparatively low because the operation and maintenance of measurement systems are more expensive and difficult in the polar regions.

There have been field campaigns to enhance observations over the polar regions. The Concordiasi field experiment over Antarctica provided additional sounding observations from more than 600 dropsondes released from 13 driftsonde-type stratospheric balloons in September and October 2010. Boullot *et al.* (2016) investigated the impact of observations on analyses and forecasts over the southern polar regions using four operational prediction systems: the Naval Research Laboratory (NRL), Global Modeling and Assimilation Office (GMAO), European Centre for Medium-range Weather Forecasts (ECMWF), and Météo-France. They examined the effects of radiosonde and dropsonde observations by computing the Forecast Sensitivity to Observations (FSO) diagnostic and conducting Observing System Experiments (OSEs). The impact of both radiosonde and dropsonde observations of temperatures at lower levels and winds at upper levels was noticeable, regardless of the system (figure 13 of Boullot *et al.*, 2016).

Previous studies have shown that the assimilation of additional radiosonde observations over the Arctic improves the forecasts of weather events like Arctic cyclones; this improvement can extend to mid-latitude regions. Inoue *et al.* (2015) showed that additional Arctic radiosonde observations from the Arctic Research Collaboration for Radiosonde Observing System Experiment (ARCROSE) could improve the prediction of a persistent strong wind event and sea-ice advection along the Northern Sea Route (NSR). The impact of additional radiosonde observations from the German research vessel, *Polarstern*, on the prediction of the Arctic cyclone in August 2012 was investigated by Yamazaki *et al.* (2015). Lee *et al.* (2019)

showed the potential benefits of adding radiosonde observations from the Korea Polar Research Institute (KOPRI) research vessel, *Araon*, in improving the weather forecasts of Alaska. Inoue *et al.* (2013) similarly found that special radiosonde launches from a research vessel in the Arctic Ocean led to forecasts that better captured an event of Arctic cyclogenesis involving a tropopause fold and that assimilation of the data removed a significant forecast temperature bias. They also found that the extra Arctic radiosondes could improve both re-analyses and forecasts beyond the immediate Arctic, with benefits to the northern half of the Northern Hemisphere. Naakka *et al.* (2019) examined the assimilation of soundings over the Arctic and found that the impact of radiosondes on analyses varied geographically. Over otherwise data-sparse areas (viz., the Arctic Ocean), the sounding data significantly improved the analyses, with their effect sometimes being greater than that of satellite observations. The effects of additional Arctic radiosonde observations on forecasts are not limited to Arctic regions. Sato *et al.* (2017) showed that extra radiosonde observations from the Norwegian young sea ICE (N-ICE2015) expedition could improve forecasts of cold-surge events over Eurasia and North America. Furthermore, Sato *et al.* (2018b) showed that additional Arctic radiosonde observations could potentially lead to improved forecasts of tropical cyclones over the North Atlantic and North Pacific. When atmospheric fields are used as external forcing for an ice–ocean coupled model, assimilation of additional radiosonde observations can improve atmospheric variables such as wind, leading to improved sea-ice forecasts (Ono *et al.*, 2016).

Recently, the importance of Arctic observations has been studied by using global and regional forecasting systems. Lawrence *et al.* (2019) assessed the impact of Arctic observations on short- and medium-range forecasts using the ECMWF system. Based on OSE results and FSO diagnostics, they found that the positive effects of Arctic observations were not limited to the Arctic, but extended to the midlatitude regions at longer lead times. They also showed that satellite microwave sounding and conventional data were the key observing systems in summer and winter, respectively. The forecast effects of Arctic observations were evaluated using a limited area model, Application of Research to Operations at Mesoscale (AROME)-Arctic, by Randriamampianina *et al.* (2021). They conducted OSEs and utilized degrees of freedom for signals and an energy norm-based approach; overall impacts of Arctic observations on analyses and forecasts of the AROME-Arctic were found to be positive, with humidity-related observations having the greatest impact.

Few studies have examined the effects of additional radiosonde observations on Antarctica analyses and forecasts. Sato *et al.* (2018a) investigated the effects

of additional radiosonde observations from the Australian research vessel *Aurora Australis* on ensemble re-analyses and forecasts, obtaining an improved prediction of upper-level troughs and Southern Hemisphere mid-latitude cyclone tracks. By assimilating extra radiosonde observations from the Japanese research vessel *Shirase* and Dome Fuji station, the central pressure of an unusually strong cyclone was reliably predicted, resulting in improved forecasts of strong winds and of moisture transport near the Antarctic coast (Sato *et al.*, 2020). Sun *et al.* (2020) demonstrated the benefits of assimilating additional radiosonde observations from the German research vessel *Polarstern* and sounding observations from unmanned aerial vehicles (UAVs). Although the assimilation impact varied for individual cases, the analyses and five-day forecasts were improved by assimilating the special observations. While not considering Antarctica itself, Soldatenko *et al.* (2018) did focus on the Southern Hemisphere, and specifically Australia, in looking at the impact of all *in-situ* observations on the Australian Bureau of Meteorology's Australian Community Climate and Earth System Simulator (ACCESS) model forecasts. Using an adjoint-based FSO approach, they were able to quantify individual observation influences. They found that the soundings assimilated, including those from Antarctic stations, were responsible for an over 10% reduction in forecast error, with the effects of radiosondes from the Antarctic stations (i.e., Casey, Davis, and Mawson) being significant. Recently, Sato *et al.* (2022) conducted OSEs to investigate the impact of Program of the Antarctic Syowa Mesosphere–Stratosphere–Troposphere/Incoherent Scatter (PANSY) radar data from the Japanese Syowa station in Antarctica on re-analyses and forecasts; they revealed that the incorporation of PANSY data reduced the ensemble spread and error over the Antarctic region and led to improved forecasts of a midlatitude cyclone over Western Australia.

The Year of Polar Prediction (YOPP) is the flagship activity of the Polar Prediction Project (PPP) of the World Meteorological Organization's World Weather Research Program (WMO's WWRP), coordinating a period of intensive observing, modeling, verification, user engagement, and education activities (Bromwich *et al.*, 2020). Recently, Bromwich *et al.* (2022) reported the impact of YOPP in the Southern Hemisphere (YOPP-SH) Special Observing Period (SOP) data using the Weather Research and Forecasting (WRF) Model over Antarctica, and they evaluated the forecasts using Automatic Weather Station (AWS), radiosonde, and ECMWF re-analysis version 5 (ERA5) data. The assimilation of the YOPP-SH radiosonde data improved lower-tropospheric temperature and upper-tropospheric wind speed forecasts. These improvements are primarily confined to regions south

of 60° S, and they are significant to the east of the Antarctic Peninsula. The experimental design in the current study is closer to operational settings than that in Bromwich *et al.* (2022) in two respects. First, in contrast to the study by Bromwich *et al.* (2022), in which analyses from three-day cycling were used as initial conditions for three-day free forecasts, extended and continuous cycling has been adopted in this study. Second, more satellite radiance observations (e.g., from hyperspectral infrared [IR] instruments) have been assimilated here. This study aims to investigate the effects of assimilating additional radiosonde observations during the YOPP-SH SOP on analyses and forecasts over Antarctica by conducting OSEs in an operational framework.

The remainder of this paper is organized as follows. Section 2 describes the observational data used for assimilation and verification. Section 3 illustrates the experimental design of the OSE. The effects of assimilation of additional radiosonde observations on analyses and forecasts are discussed in Section 4, and finally, Section 5 provides a summary and conclusions.

2 | DATA AND METRICS

The SOP of the YOPP-SH was from November 16, 2018 to February 15, 2019, and in this period radiosonde and drifting buoy observations were enhanced (Bromwich *et al.*, 2020). In this study, the effects of radiosonde observations on analyses and forecasts over Antarctica were investigated by conducting DA cycling experiments. Figure 1 shows the number of routine and YOPP-SH special observations at 0000, 0600, 1200, and 1800 UTC. Routine radiosonde launches were mainly conducted at 0000 and 1200 UTC (except Mario Zucchelli at 0600 UTC) and concentrated over the coastal regions of Antarctica (except South Pole and Dome C). YOPP-SH radiosonde observations filled the gaps in time and space; thus, observations at 0600 and 1800 UTC and observations over inland regions (e.g., Antarctic Plateau) were increased. The number of additional radiosonde launches during the SOP was 2,244, more than double that of routine radiosonde launches. There were still fewer radiosonde observations over the western and inland regions of Antarctica than in the eastern and coastal regions even during the SOP. The observations from both routine and YOPP-SH SOP launches were assimilated and used for verification in this study.

The number of AWSs over Antarctica is more than 160; their distribution is shown in Figure 2 of Bromwich *et al.* (2020). AWS observations transmitted to the global telecommunication system (GTS), included in the Prepared Binary Universal Form for the Representation of meteorological data (PrepBUFR)-format files distributed

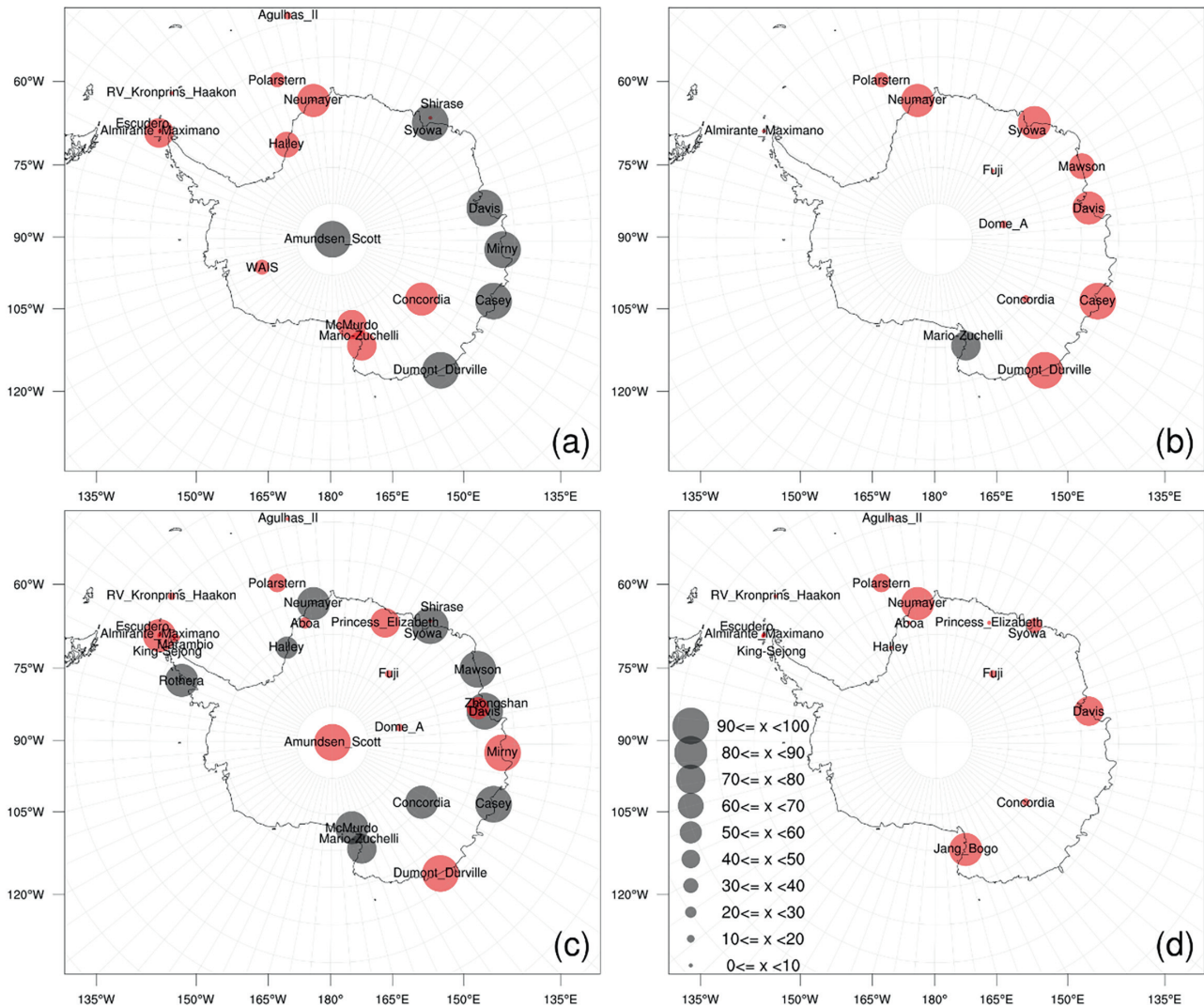


FIGURE 1 The number of radiosonde launches at (a) 0000 UTC, (b) 0600 UTC, (c) 1200 UTC, and (d) 1800 UTC during YOPP-SH SOP (i.e., from 0000 UTC 15 November 2018 to 0000 UTC 15 February 2019). Size of a circle for each station is proportional to the number of launches, and color of the circle denotes routine (black) and YOPP-SH SOP special (red) observations.

by the National Centers for Environmental Prediction (NCEP), were assimilated. To verify the forecasts, AWS observations from the Antarctic Meteorological Research Center (AMRC) of the University of Wisconsin-Madison were used together with AWS observations in PrepBUFR files. The distributions are shown later in Figure 9 below.

To quantify the effects of additional radiosonde observations, two metrics, the difference in root mean square error and total energy of error (dRMSE and TEE, respectively), are defined as follows:

$$\text{dRMSE}(\%) = \frac{\text{RMSE}_{\text{CTL}} - \text{RMSE}_{\text{YOPP}}}{\text{RMSE}_{\text{CTL}}} \times 100 \quad (1)$$

where RMSE_{CTL} and $\text{RMSE}_{\text{YOPP}}$ are the errors of the control (CTL) and YOPP experiments, respectively. The dRMSE denotes the extent to which the RMSE of the

analysis or forecast is reduced by assimilating additional radiosonde observations.

Following the definitions of the moist total energy of singular vector (Ehrendorfer *et al.*, 1999) and difference total energy (Zhang *et al.*, 2003), TEE is defined.

$$\text{TEE} = \frac{1}{2} \frac{1}{A} \sum_{i,j,k} \left(u'^2_{ijk} + v'^2_{ijk} + \frac{c_p}{T_r} T'^2_{ijk} + \frac{L^2}{c_p T_r} q'^2_{ijk} \right) \quad (2)$$

where u , v , T , and q represent zonal wind, meridional wind, temperature, and water vapor mixing ratio, and a prime denotes an error of each variable. Subscripts i , j , and k indicate zonal, meridional, and vertical directions, respectively, and A denotes an area of the horizontal domain. c_p is the specific heat at constant pressure ($1005.7 \text{ J} \cdot \text{kg}^{-1} \cdot \text{K}^{-1}$), T_r is the reference temperature (270 K), and L is the latent heat of condensation per

unit mass ($2.5104 \times 10^6 \text{ J} \cdot \text{kg}^{-1}$). The TEE metric represents vertically integrated and horizontally averaged moist total energy of the error for analyses or forecasts; hence reduction of the error through the assimilation of additional radiosonde observations can be quantified by comparing the TEE metrics from the CTL and YOPP experiments.

3 | EXPERIMENTAL DESIGN

An OSE is a method to investigate the effects of assimilating a specific observation type on the quality of analyses and/or forecasts. In the OSE framework, one type of observation is excluded (or included) when all the available observations are assimilated. In this study, we conducted two experiments: in one, “CTL,” only routine radiosonde observations were assimilated, and in the other, “YOPP,” radiosonde observations from YOPP-SH SOP were additionally assimilated. Note that the other conventional observations (e.g., aircraft and buoy), Global Positioning System Radio Occultation (GPS RO) observations, and satellite radiance observations were assimilated in both experiments.

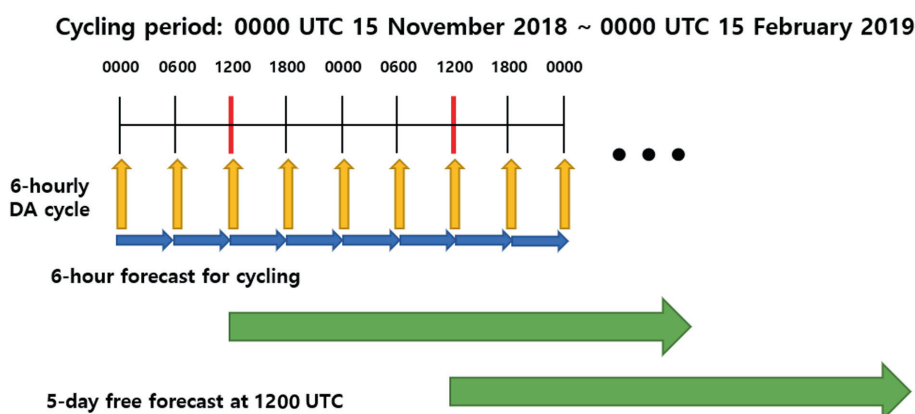
In the CTL and YOPP experiments, a six-hour forecast from the previous cycle acts as a background for the current cycle (i.e., a warm start), except for the very first cycle (i.e., a cold start). The cycling period was from 0000 UTC 15 November 2018 to 0000 UTC 15 February 2019, with a cycling interval of six hours. At 1200 UTC on each day, a five-day forecast starting from the analysis was made using the WRF model. A schematic of the DA cycling experiment is shown in Figure 2.

WRF Version 4.1.5 (Skamarock *et al.*, 2019) was used to conduct both six-hour forecasts for DA cycling and five-day free forecasts every 1200 UTC. Figure 3 shows the geographical areas of the three two-way nested domains. Domain 1 covers the Antarctic continent and the surrounding ocean, and domains 2 and 3 focus on

the Antarctic Peninsula and King George Island, respectively. The horizontal resolutions of domains 1, 2, and 3 were 27, 9, and 3 km, respectively, and the number of vertical levels for all domains was 61, with a model top at 10 hPa. Note that DA was conducted only on domain 1, and analyses and forecasts from domain 1 were used for verification/analyses in this study; results from domains 2 and 3 will be explored in future work. The NCEP Global Forecast System (GFS) analyses and forecasts were used for the background only at the very first cycle and lateral boundary conditions for six-hour and five-day forecasts, respectively. The following physics schemes were selected to run the WRF model: WRF Single Moment 5-class (WSM5) microphysics (Hong *et al.*, 2004), Grell-Freitas cumulus (Grell and Freitas, 2014), Mellor–Yamada–Janjic (MYJ) planetary boundary layer (Janjic, 1994), Rapid Radiative Transfer Model for GCM (RRTMG) longwave and shortwave radiation (Iacono *et al.*, 2008), and the Noah land surface model (LSM; Tewari, 2004) schemes.

Background error covariances for the DA system were computed using the National Meteorological Center (NMC) method (Parrish and Derber, 1992), that is, using statistics from the differences between 24-hr and 12-hr forecasts of a two-month period (December 2018 and January 2019). Conventional observations, such as observations from radiosonde, aircraft, land station, ship, buoy, satellite-derived wind observations, GPS RO refractivity observations, and satellite radiance observations from IR and microwave (MW) instruments, were assimilated using the three-dimensional variational (3D-Var) DA method in the WRF Data Assimilation (WRFDA) system (Barker *et al.*, 2012). Radiance assimilation details (e.g., satellites/sensors, observation operator, bias correction, and quality control) are summarized in Table 1. Horizontal distributions of radiosonde, aircraft, land-surface, ship, satellite-derived wind, and GPS RO refractivity observations assimilated in the YOPP experiment at 1200 UTC 10 January 2019 are shown in Supplementary Figure S1.

FIGURE 2 Schematic diagram for data assimilation cycling experiments. Cycling period is from 0000 UTC 15 November 2018 to 0000 UTC 15 February 2019, and cycling interval is six hours. Orange arrows indicate six-hourly assimilations, and blue arrows indicate six-hour forecasts for cycling, at 0000, 0600, 1200, and 1800 UTC. Green arrows denote five-day forecasts starting at 1200 UTC. [Colour figure can be viewed at wileyonlinelibrary.com]



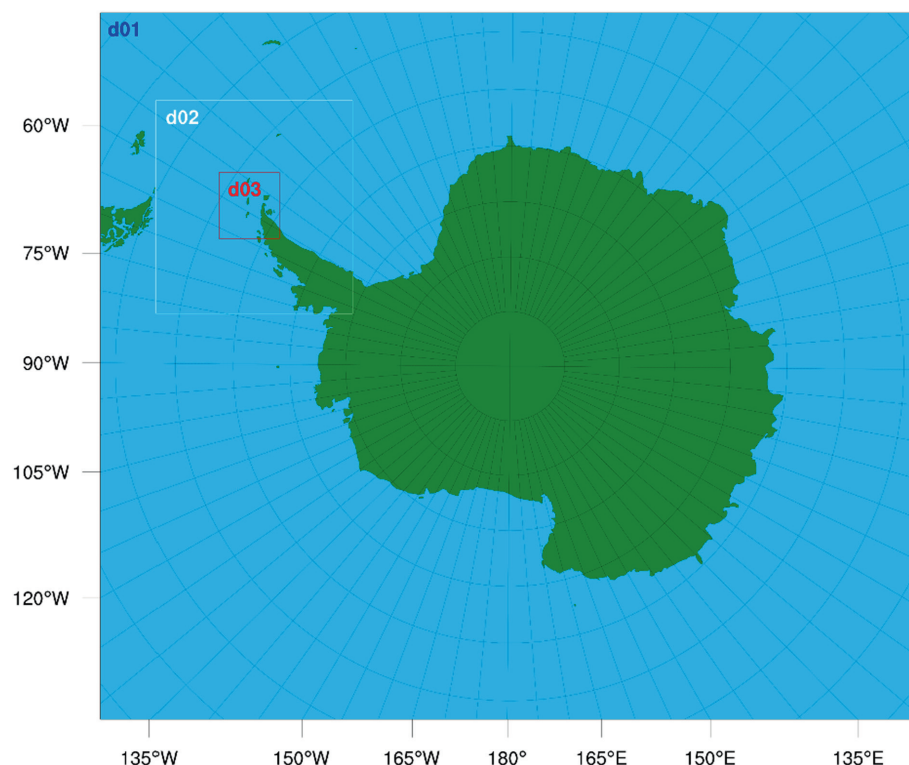


FIGURE 3 Geographical areas of domains 1, 2, and 3. [Colour figure can be viewed at wileyonlinelibrary.com]

TABLE 1 Details of radiance data assimilation.

Sensors	Infrared	AIRS from aqua satellite IASI from MetOp-A, B satellitess AMSU-A from NOAA-15, 18, 19, MetOp-A, B, aqua satellitess MHS from NOAA-19, MetOp-A, B
	Microwave	
Observation operator		Community Radiative Transfer Model (CRTM; Han <i>et al.</i> , 2006)
Bias correction		Variational Bias Correction (VarBC; Dee, 2004)
Quality control		QC procedures in WRFDA (Liu <i>et al.</i> , 2012)

Even with the additional YOPP-SH SOP radiosonde observations, radiosonde observations are sparse, especially over the western and inland regions of Antarctica. Surface observations are also sparsely distributed over Antarctica, except around the Antarctic Peninsula. Although polar-orbiting satellites provide radiance observations over the southern polar region, only a subset of them can be assimilated. For example, channels that are sensitive to the surface and whose peaks of weighting functions is above the model top are excluded. Additionally, pixels (i) affected by cloud or precipitation, (ii) over ice and snow surfaces, and (iii) over high-topography regions are not assimilated. As an example, at 1200 UTC 10 January 2019, only approximately 16%, 29%, 3%, and 14% of the total radiance observations from the AMSU-A, MHS, AIRS, and IASI instruments are assimilated. As mentioned, the only difference between the CTL and YOPP experiments was whether additional YOPP-SH radiosonde observations were assimilated.

4 | EFFECTS OF YOPP-SH RADIOSONDE OBSERVATIONS

4.1 | Effects on analyses

DA attempts to produce an analysis that is a statistically optimal combination of the background (or first guess) field and observations. In line with the definition of DA, O-B (observation minus background) and O-A (observation minus analysis) statistics are widely used in analyses of the DA process. Figure 4 shows the RMS of O-B and O-A for zonal wind, meridional wind, temperature, and water vapor mixing ratio from radiosonde observations, together with the number of assimilated observations. The RMS of O-B (O-A) is calculated using differences between the observation and background (analysis) from all observation locations and levels. In the CTL and YOPP experiments, O-A is smaller than O-B for all variables and at all cycles. This implies that the assimilation of radiosonde

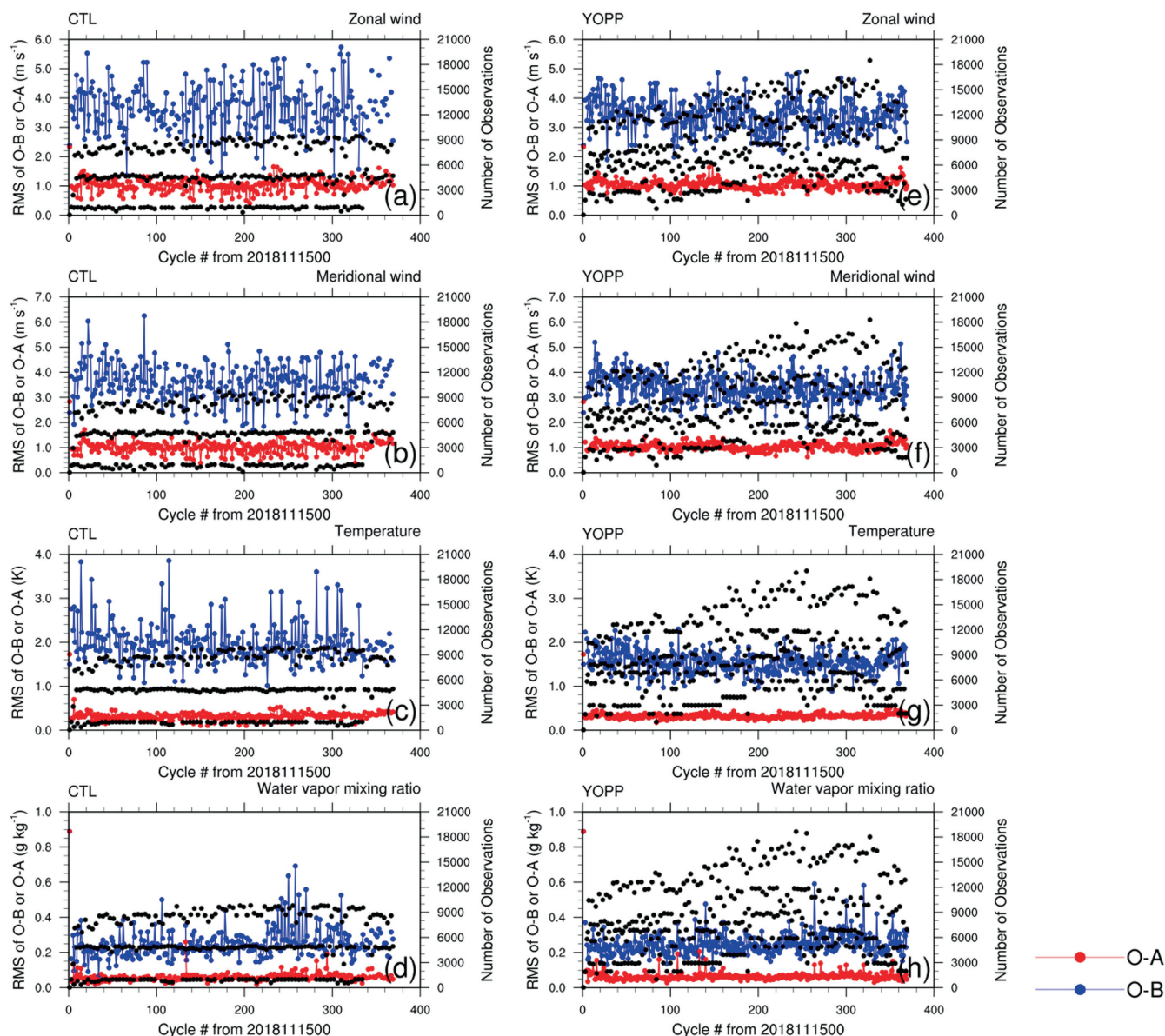


FIGURE 4 Root mean square (RMS) of O-B (observation minus background, blue) or O-A (observation minus analysis, red) together with the number of assimilated observations (black) for (a) zonal wind (m s^{-1}), (b) meridional wind (m s^{-1}), (c) temperature (K), and (d) water vapor mixing ratio (g kg^{-1}) of CTL experiment, as a function of data assimilation cycle. (e–h) Same as (a–d) except for YOPP experiment.

observations is successful in both experiments. The number of assimilated observations in the CTL experiment varies with the time of day (i.e., 0000, 0600, 1200, and 1800 UTC), a general characteristic of radiosonde observations. In the YOPP experiment, the temporal variation in the number of assimilated observations is significantly reduced, and the number of assimilated observations is nearly doubled compared to that in the CTL experiment. Owing to the enhanced radiosonde observations, the temporal fluctuation of O-B values decreases in the YOPP experiment. Temporal standard deviations of O-B for zonal wind, meridional wind, temperature, and water vapor mixing ratio in the YOPP experiment are approximately

0.56 m s^{-1} , 0.53 m s^{-1} , 0.24 K , and 0.07 g kg^{-1} , respectively, which are smaller than those in the CTL experiment (0.81 , 0.71 , 0.45 , and 0.09). Additionally, temporal means of O-B for zonal wind, meridional wind, temperature, and water vapor mixing ratio in the YOPP experiment are reduced by about 7%, 6%, 21%, and 4%, compared to the CTL experiment.

Figure 5 shows the vertical distributions of the analysis increment (A-B; analysis minus background) for zonal wind, meridional wind, temperature, and water vapor mixing ratio. Analysis increments are spatially averaged over domain 1 and also averaged in time over the cycling period. Analysis increments reflect biases in the background (here

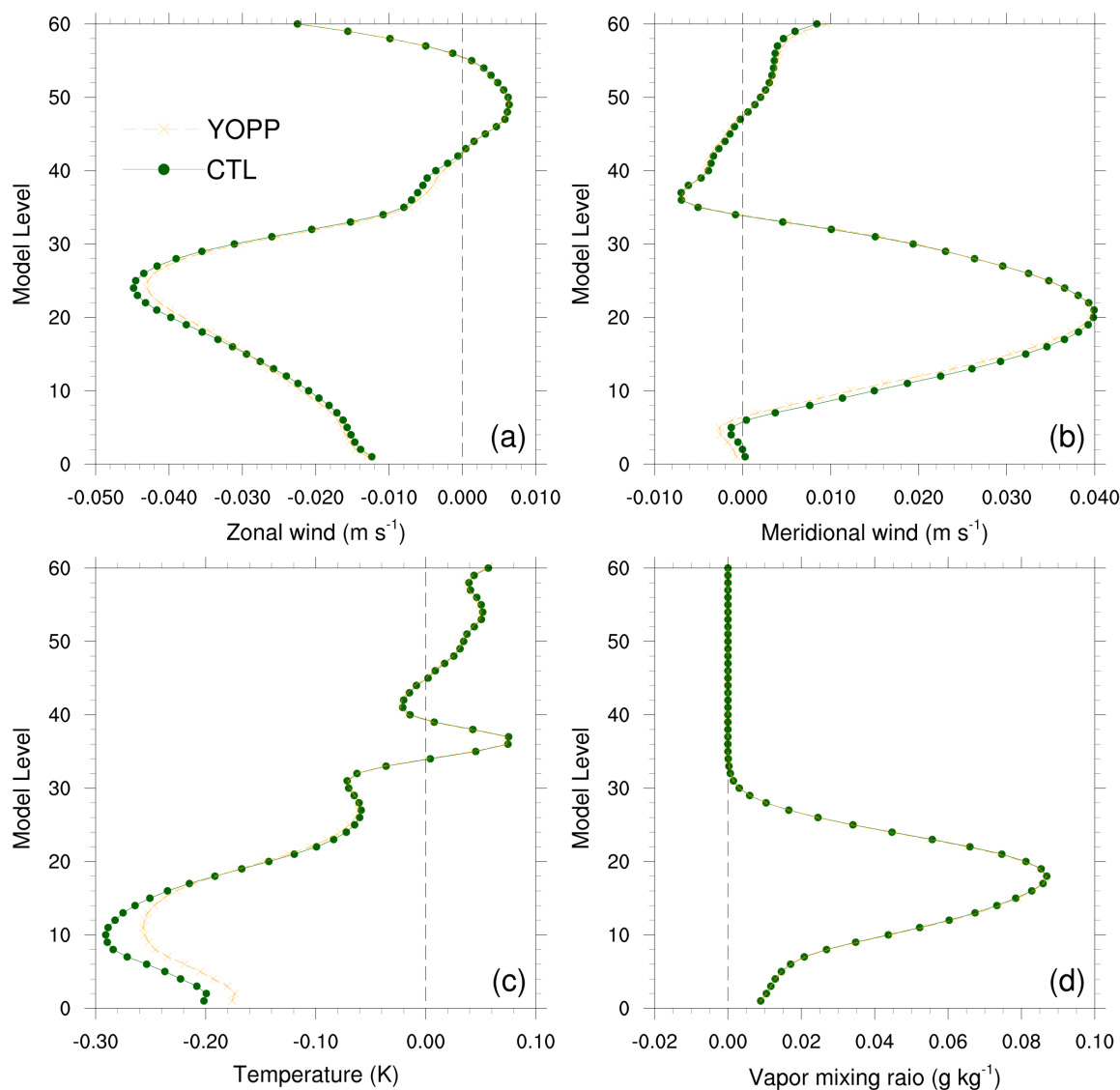


FIGURE 5 Vertical distributions of mean analysis increments for (a) zonal wind (m s^{-1}), (b) meridional wind (m s^{-1}), (c) temperature (K), and (d) water vapor mixing ratio (g kg^{-1}) of CTL (green solid line with circle) and YOPP (orange dashed line with cross) experiments. For each level, analysis increments are averaged over domain 1, and then they are averaged over the cycling period. [Colour figure can be viewed at [wileyonlinelibrary.com](https://onlinelibrary.wiley.com/doi/10.1002/qj.4528)]

a short-range forecast) because DA tries to rectify background biases by taking advantage of the observations. Analysis increments for zonal wind and temperature are negative at almost all model levels; in contrast, those for meridional wind and water vapor mixing ratio are positive at most model levels. Therefore, in the background, the zonal wind is stronger and the meridional wind is weaker than in the observations. In addition, background temperatures are warmer and water vapor amounts are less than in the observations. Compared to that in the CTL experiment, the absolute magnitude of analysis increment is reduced in the YOPP experiment, especially for temperature at lower-tropospheric levels (viz 850–925 hPa). This is because the background in the

YOPP experiment is continuously improved by assimilating more observations as DA cycles go on.

Usually, independent (re)analyses and observations not assimilated are used to verify the analyses. Additionally, own analysis and observations assimilated can be used to verify forecasts. Because the number of observations over polar regions is less than that over mid-latitude or tropical regions, re-analyses for the polar regions potentially have greater errors. Previous studies have confirmed the reliability of the ECMWF ERA5 re-analysis both over the Arctic (Graham *et al.*, 2019a,b; Wang *et al.*, 2019; Gu *et al.*, 2021; Yu *et al.*, 2021) and over Antarctica (Gossart *et al.*, 2019; Tetzner *et al.*, 2019; Dong *et al.*, 2020; Zhu *et al.*, 2021; Harrison *et al.*, 2022;

Xin *et al.*, 2023) in representing key atmospheric variables such as wind, temperature, and moisture. On the basis of previous studies, we decided to use the ERA5 re-analysis as a reference for verifying analyses and forecasts. To supplement the verification using ERA5, we additionally verified forecasts against radiosonde observations. Note that care should be taken when the difference between the re-analysis data and analyses (or forecasts) is small because the re-analysis data have a certain level of error.

Figure 6 shows the difference in RMSE between the CTL and YOPP experiments (i.e., CTL minus YOPP) for 850-hPa temperature, 500-hPa geopotential height, and 200-hPa zonal wind during the cycling period. RMSEs are calculated against ERA5 re-analysis over domain 1. The red bar indicates that RMSEs are reduced in the YOPP experiment compared to those in the CTL experiment, and vice versa for the blue bar. For 850-hPa temperature, compared to that in the CTL experiment, the RMSE is substantially decreased in YOPP for most of the DA cycles (viz about 88% of total cycles), and the averaged difference in RMSE of improved cycles (0.14 K) is greater than that of degraded cycles (−0.05 K) in an absolute sense. Analyses of the 500-hPa geopotential height of the YOPP experiment are enhanced compared to those of CTL for about 66% of the total cycles. An absolute value of the averaged difference in RMSE from improved cycles (1.59 m) is larger than that from degraded cycles (−1.03 m). Finally, an improvement in 200-hPa zonal wind analyses of the YOPP experiment is not as noticeable as the aforementioned variables. For about 60% of the total cycles, the RMSEs of the YOPP experiment are reduced compared to those of the CTL experiment, and the averaged difference in RMSE of improved cycles (0.14 m s^{−1}) is slightly bigger than that of degraded cycles (−0.12 m s^{−1}) in an absolute manner. Moreover, averaged differences in RMSE over all cycles for 850-hPa temperature, 500-hPa geopotential height, and 200-hPa zonal wind are all positive (0.12 K, 0.69 m, and 0.04 m s^{−1}, respectively), and all differences are statistically significant at the 90% confidence level.

The same analysis as in Figure 6 was conducted for two regions, namely south of 60° S and north of 60° S (Supplementary Figures S2 and S3), instead of the whole domain. Qualitatively, the conclusions drawn from Figure 6 can be applied to both regions. However, the effects of additional radiosonde observations on analyses for south of 60° S are much larger than those for north of 60° S, which is consistent with results from Bromwich *et al.* (2022). Averaged differences over all cycles of 850-hPa temperature, 500-hPa geopotential height, and 200-hPa zonal wind are positive and statistically significant at the 90% level for south of 60° S, but averaged difference of only 850-hPa temperature is positive and statistically significant for north of 60° S.

This is because most of the additional radiosonde observations are located south of 60° S.

In summary, the assimilation of the YOPP-SH SOP radiosonde observations improves the quality of the analyses, and the improvement is most significant in the temperature variable at lower-tropospheric levels (viz., for 850 hPa and below).

4.2 | Effects on forecasts

As stated in Section 3, the observations, including those from the special radiosondes, are assimilated every six hours during the cycling period, and five-day WRF forecasts are conducted at 1200 UTC daily. A total of 92 forecasts for each experiment (CTL or YOPP) are verified against ECMWF ERA5 re-analyses, radiosonde observations, and AWS observations. Note that radiosonde and AWS observations, assimilated in both experiments, are used to verify forecasts as the forecasts (not the analyses) are independent of these observations.

Figure 7 shows the dRMSE between CTL and YOPP experiments for zonal wind, meridional wind, temperature, and geopotential height. RMSEs are calculated against ERA5 re-analysis over domain 1 and averaged using the 92 forecasts. Compared to those in the CTL experiment, the temperature forecasts are improved in the YOPP experiment at almost all levels and for nearly all lead times, with a maximum dRMSE of approximately 3.5%. Forecast improvement in the YOPP experiment is statistically significant at a 90% confidence level, up to about a 42-hr lead time at the 850-hPa level. At the 925- and 500-hPa levels, the improvement is statistically significant up to about 21-hr and 24-hr lead times, respectively. The improvement at 700-hPa and 300-hPa levels is also statistically significant for some lead times. Except at the 1,000-hPa level and for longer lead times (i.e., longer than 108 hours), the predictability of geopotential height in the YOPP experiment is substantially increased compared to that in the CTL experiment, with a maximum dRMSE of approximately 3.9%. The forecast improvement at 700-hPa and 500-hPa levels is statistically significant even for 45-hr and 48-hr lead times, respectively. Some statistically significant improvements are also found at the 300 hPa level.

For zonal wind and meridional wind, the forecasts in the YOPP experiment are better than those in the CTL experiment, mainly at upper levels (i.e., higher than 200 hPa), with a maximum dRMSE of approximately 2.5% and approximately 2.0%, respectively. The improvement of zonal wind forecasts is statistically significant between six-hour (15-hr) and 45-hr (45-hr) lead times at the 100-hPa (50-hPa) level. Although the improvement

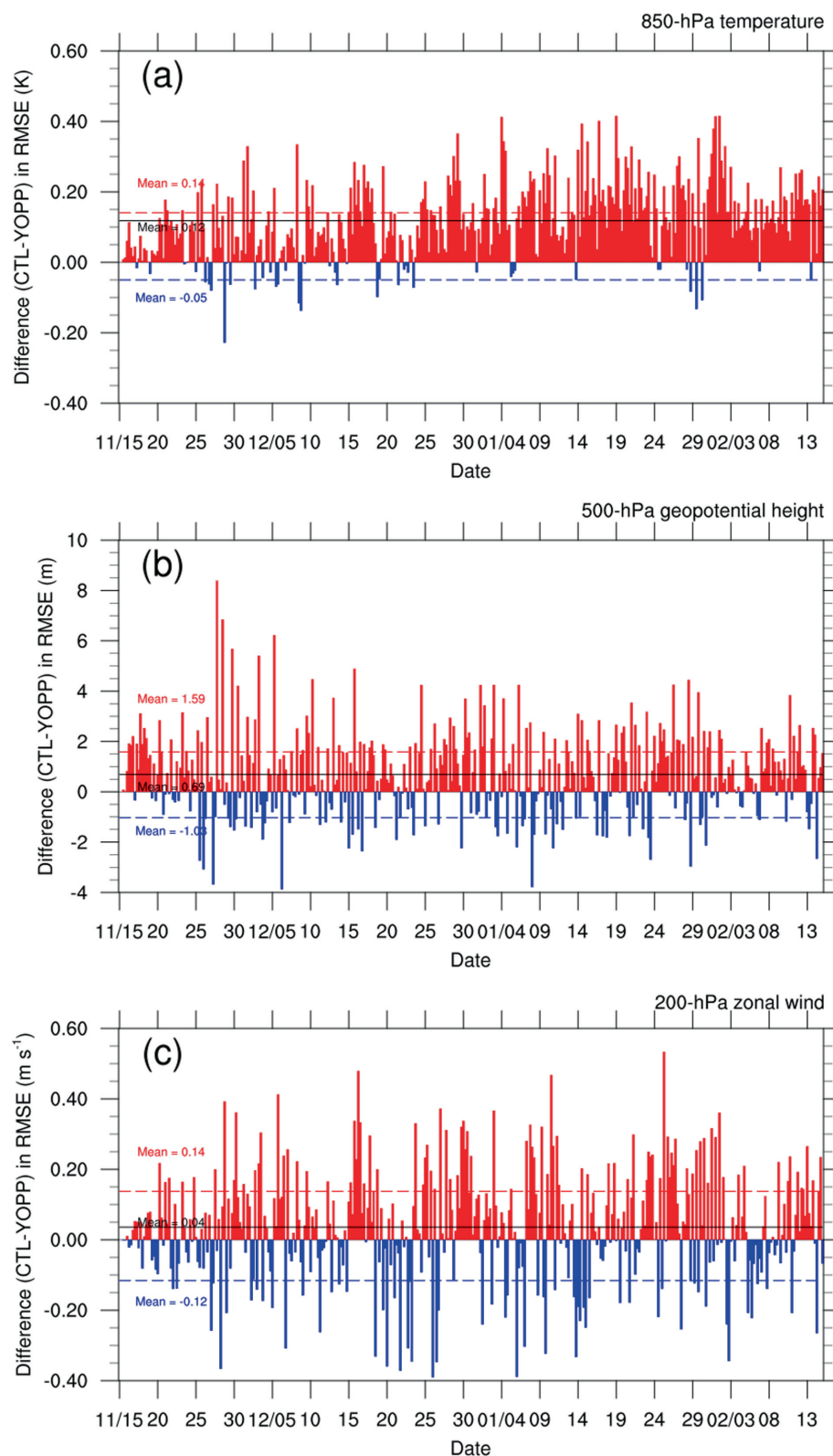


FIGURE 6 Differences in root mean square error (RMSE) of (a) 850-hPa temperature (K), (b) 500-hPa geopotential height (m), and (c) 200-hPa zonal wind (m s^{-1}) between CTL and YOPP experiments (CTL minus YOPP) during the cycling period. RMSEs of analyses are calculated against ERA5 re-analysis over domain 1. Red (blue) dashed line indicates an average of differences in RMSE from the cycles when RMSE is reduced (increased) in the YOPP experiment compared to the CTL experiment. An average of differences in RMSE over all cycles is indicated by black solid line when it is statistically significant at the 90% confidence level. [Colour figure can be viewed at [wileyonlinelibrary.com](https://onlinelibrary.wiley.com/doi/10.1002/qj.4528)] [wileyonlinelibrary.com](https://onlinelibrary.wiley.com/doi/10.1002/qj.4528)]

of meridional wind forecasts is less than that of zonal wind forecasts, the improvement at the 100-hPa level is statistically significant between six-hour and 33-hr lead times. Forecasts of the water vapor mixing ratio in the YOPP experiment are improved at the 925-hPa level up

to about a 66-hr lead time. However, the improvement is not statistically significant at the 90% level (not shown). To sum up, through the assimilation of the additional YOPP-SH radiosonde observations, the forecasts of temperature, geopotential height, and zonal/meridional wind

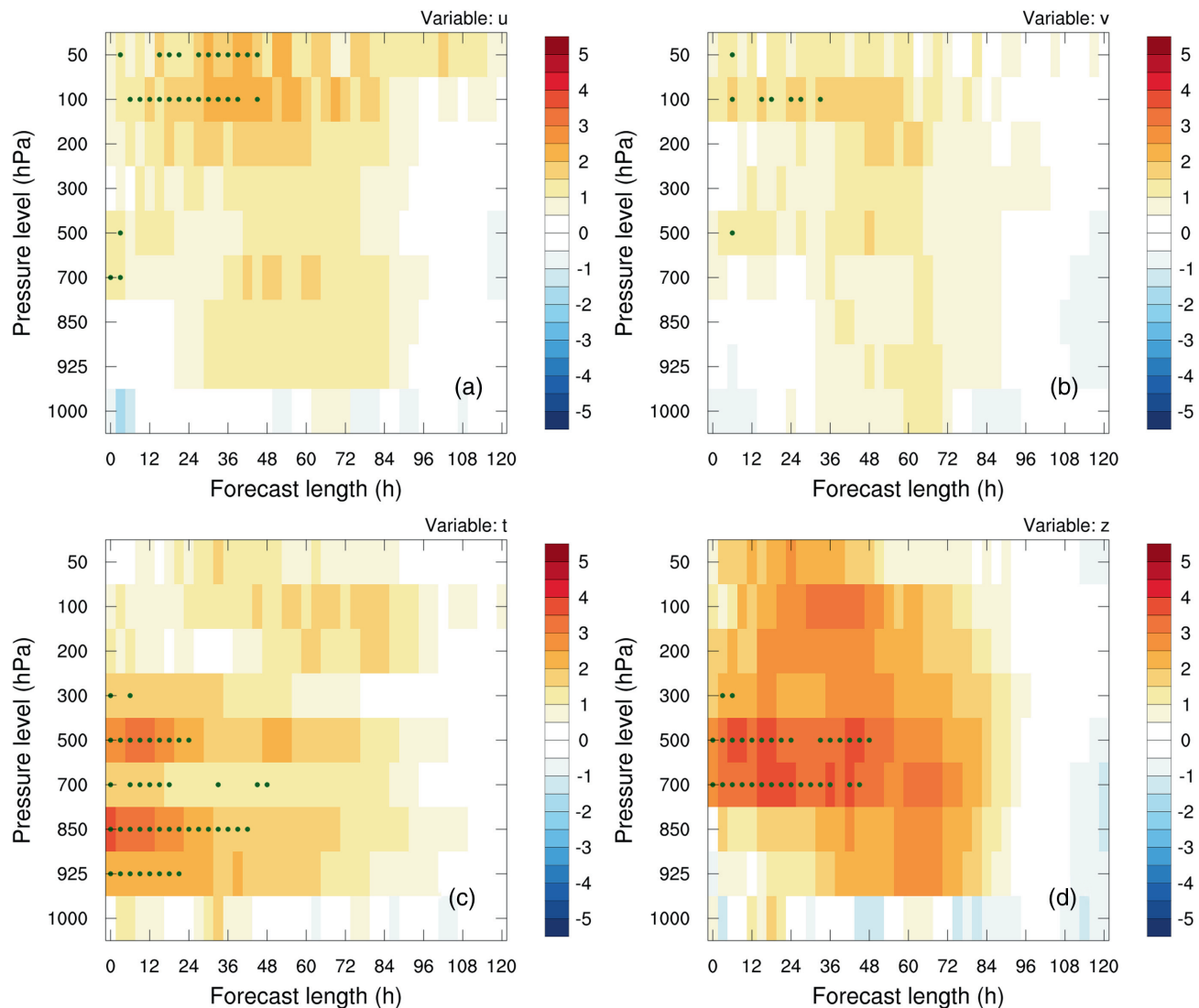


FIGURE 7 Percentage difference in root mean square error (dRMSE, %) between CTL and YOPP experiments (CTL minus YOPP) for (a) zonal wind, (b) meridional wind, (c) temperature, and (d) geopotential height. RMSE is computed against ERA5 re-analysis over domain 1. Green dots denote statistical significance at the 90% confidence level, computed through a bootstrap resampling method.

are improved in the YOPP experiment, compared to those in the CTL experiment, with improvements in the lower, middle, and upper levels, respectively. The gain in the forecast lead time is nearly 48 hours for temperature and geopotential height.

The same analysis as in Figure 7 was done for two specific regions: south of 60° S and north of 60° S (Supplementary Figures S4 and S5). Qualitatively, the results for two regions agree with those for the whole domain. Forecasts of mass variables (i.e., temperature and geopotential height) at lower and mid-levels are improved initially, while forecasts of wind variables at upper levels are improved later in the YOPP experiment. However, the effects of assimilating additional radiosonde observations from the region south of 60° S, where most additional radiosonde observations are located, are much greater

than those from the region north of 60° S. This is consistent with results from Bromwich *et al.* (2022).

Forecasts from the CTL and YOPP experiments are verified against radiosonde observations (both routine and YOPP-SH SOP observations) to examine whether the overall verification results using ERA5 re-analyses and radiosonde observations are consistent. Figure 8 shows the vertical distributions of the mean absolute errors (MAEs) of the CTL and YOPP experiments for zonal wind, meridional wind, temperature, and water vapor mixing ratio. MAEs are computed using radiosonde observations and 24-hr forecasts, and they are averaged over the cycling period. The shape of the vertical distribution of the MAEs for the YOPP experiment is similar to that for the CTL experiment, regardless of the variables. For temperature, the MAEs of the YOPP experiment are smaller than those

of CTL at all pressure levels. The forecast improvement at the 925-, 850-, and 300-hPa levels is statistically significant at the 90% confidence level. The MAEs of the water vapor mixing ratio for the YOPP experiment are less than those for CTL at pressure levels below 300 hPa, except at 1,000 hPa, and the differences between the CTL and YOPP experiments are statistically significant at the 925-hPa level. For zonal wind, the 24-hr YOPP forecasts are improved compared to the CTL forecasts at all pressure levels except at levels higher than 20 hPa. The improvement is statistically significant at the 400-, 300-, and 200-hPa levels. Finally, the meridional wind forecasts of YOPP are enhanced compared to those of CTL at nearly all pressure levels (cf., the 1,000-hPa level). However, the enhancement is not statistically significant at the 90% level. In short, the 24-hr forecasts of the YOPP experiment are better than those of the CTL experiment at most pressure levels, regardless of the variables. The forecast improvement is statistically significant at lower-tropospheric levels for temperature and water vapor and at upper-tropospheric and lower-stratospheric levels for zonal wind. The verification results using radiosonde observations are qualitatively consistent with those obtained using the ERA5 re-analyses. Some differences (e.g., levels where statistically significant forecast improvements appear) between them are due to inhomogeneity in the radiosonde horizontal distribution (i.e., radiosonde sites are concentrated in the coastal regions of Antarctica).

Forecasts of surface variables are critical because they provide essential information for logistics, research activities, and station operations. Figure 9 shows the horizontal distributions of dRMSE between CTL and YOPP for 12–33-hr forecasts of zonal wind, meridional wind, temperature, and water vapor mixing ratio. The RMSEs are calculated against AWS observations over Antarctica and averaged over the cycling period. At approximately three-fourths of all AWSs, forecasts of temperature are improved in the YOPP experiment compared to those in the CTL experiment. The temperature forecasts of YOPP are better than those of CTL, mostly over the coastal regions of Antarctica, especially near Queen Maud Land. The forecast improvement from eight AWS locations is statistically significant at the 90% confidence level, with a maximum dRMSE of 15.1%. The forecasts of the water vapor mixing ratio in YOPP are better than those in CTL at approximately 75% of the AWSs used for verification. As with temperature, water vapor forecasts are enhanced in the YOPP experiment over coastal regions compared to those in CTL. At AWS locations over Queen Maud Land, Antarctic Peninsula, and Casey (Dome A), the forecast improvement (degradation) in YOPP is statistically significant, with a maximum (minimum) dRMSE of 17.0% (−13.8%). The number of AWSs

where zonal wind forecasts of YOPP are improved over CTL is nearly the same as the number of stations where the opposite is true. In the case of the zonal wind, the forecast is improved (degraded) at three (one) stations, namely Halley, Novolazarevskaya, and WAIS (Zhongshan), with statistical significance at the 90% level. Similar to the zonal wind, meridional wind forecasts in YOPP are better than those in CTL at approximately half of the total AWSs. The forecast improvement (degradation) at AWSs near Neumayer (Dumont D'Urville) is statistically significant at the 90% confidence level. In brief, the effects of assimilating additional YOPP-SH radiosonde observations on surface-variable forecasts are positive for temperature and water vapor mixing ratio, but marginal for the wind components. In comparison with inland regions of Antarctica, over coastal regions, surface-variable forecasts of the YOPP experiment are improved over those of the CTL experiment, and statistically significant improvement is mostly found over the coastal regions. This is because most of the additional radiosonde observations are over coastal regions.

Overall, based on verification against ERA5 re-analyses and radiosonde/AWS observations, the forecasts of the YOPP experiment, where additional YOPP-SH radiosonde observations are assimilated, are better than those of the CTL experiment, where only routine radiosonde observations are assimilated. In particular, the forecasts of temperature and water vapor mixing ratio variables are improved at lower-tropospheric levels. On the other hand, for wind, forecasts are improved at upper-tropospheric levels. The assimilation of the additional radiosonde observations leads to a gain in the forecast lead time with the gain being dependent on variable and level. In addition, the effects of additional radiosonde observations on forecasts are much larger for south of 60° S than north of 60° S. Forecasts of surface variables, especially temperature and water vapor variables over coastal regions, are improved from the extra sounding assimilation. These results are consistent with those of Bromwich *et al.* (2022). Note that the impact of the assimilation of YOPP-SH SOP observations for a specific period (i.e., January 1–17, 2019) considered in Bromwich *et al.* (2022) is greater than that for the whole SOP (not shown).

4.3 | Spreading of effects

Both the routine and YOPP-SH SOP radiosonde observations are concentrated over the coastal regions and the eastern parts of Antarctica (Figure 1). In this section, by defining the TEE, we investigate how the effects of assimilating additional observations spread in the longitudinal, latitudinal, and vertical directions.

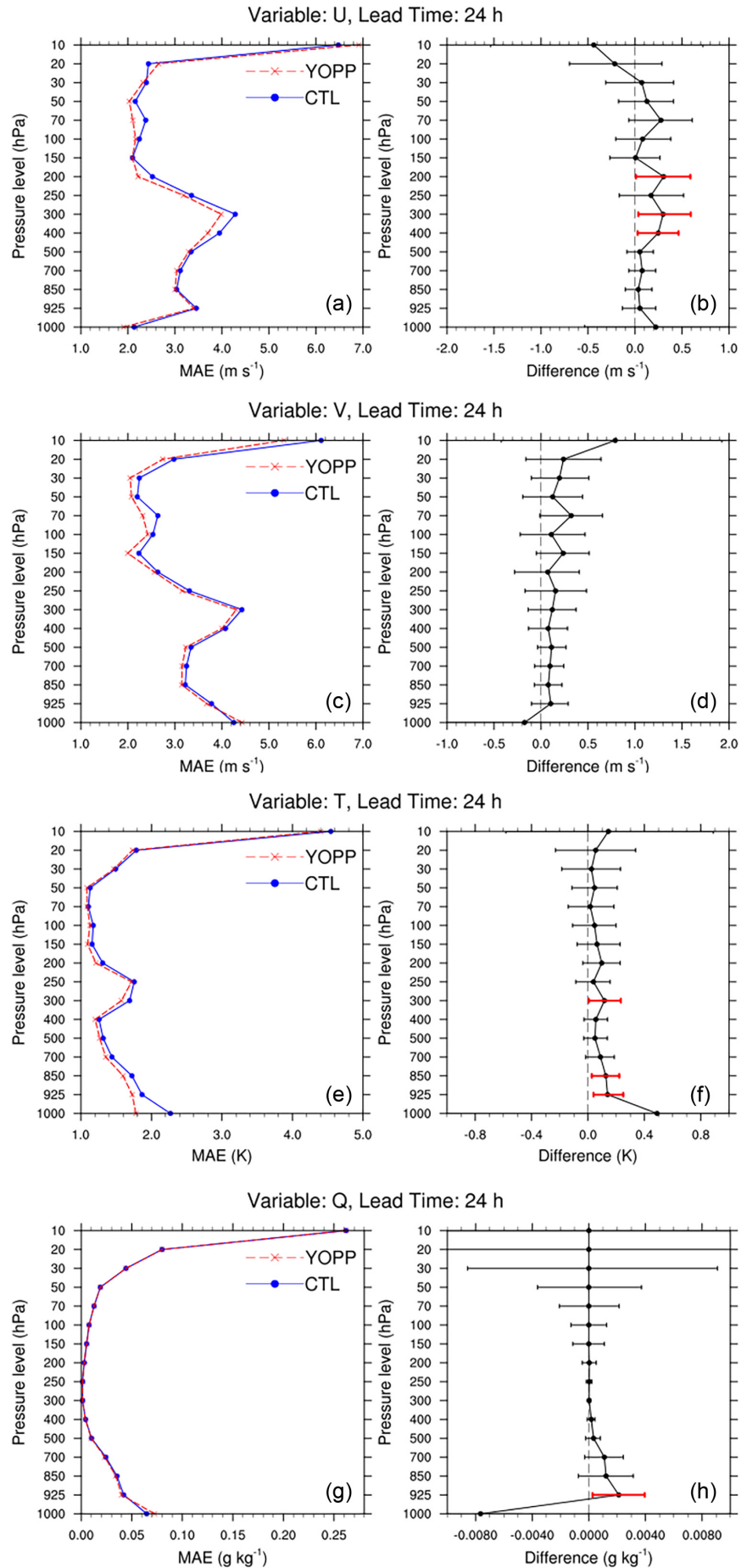


FIGURE 8 Vertical distributions of mean absolute errors (MAEs) for 24-hr forecasts of (a) zonal wind (m s^{-1}), (c) meridional wind (m s^{-1}), (e) temperature (K), and (g) water vapor mixing ratio (g kg^{-1}) in CTL (blue solid line with circle) and YOPP (red dashed line with cross). Errors are calculated against radiosonde observations, and averaged over the cycling period. Differences in MAE between CTL and YOPP (CTL minus YOPP) experiments for (b) zonal wind, (d) meridional wind, (f) temperature, and (h) water vapor mixing ratio. Error bars for the differences are computed using a bootstrap method, and red color means that the difference is statistically significant at the 90% confidence level. [Colour figure can be viewed at wileyonlinelibrary.com]

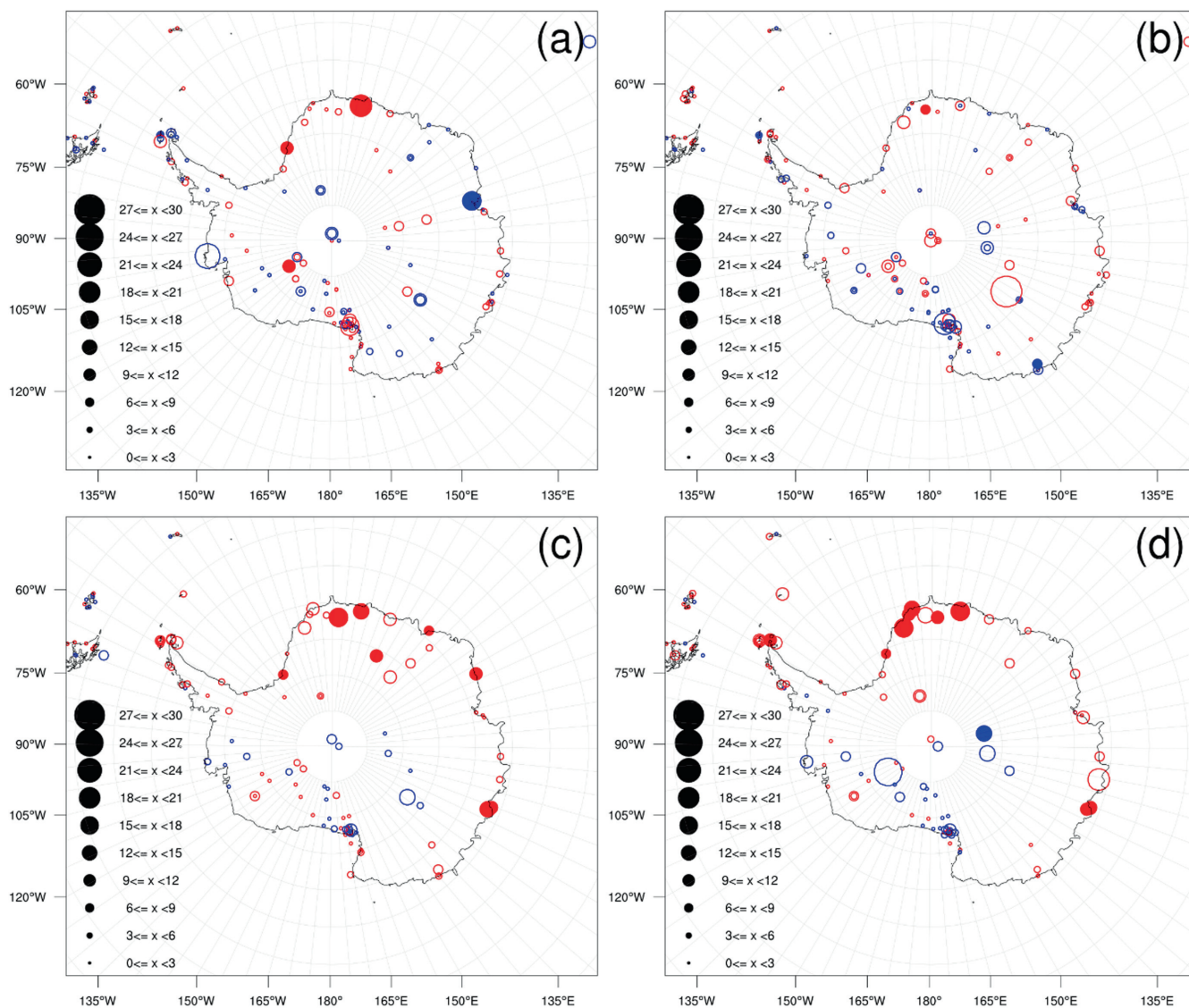


FIGURE 9 Horizontal distributions of percentage difference in root-mean-square error (dRMSE, %) between CTL and YOPP experiments (CTL minus YOPP) for 12–33-hr forecasts of (a) zonal wind, (b) meridional wind, (c) temperature, and (d) water vapor mixing ratio. RMSEs are calculated against automatic weather station (AWS) observations, and averaged over the cycling period. Size of circles is proportional to dRMSE, and red (blue) circles denote forecast improvement (degradation) in the YOPP experiment. Statistical significance is calculated using a bootstrap resampling method, and filled circles denote statistically significant differences at the 90% confidence level.

Figure 10 shows horizontal distributions of sea level pressure (SLP) and streamlines at 10 m, averaged over the cycling period (i.e., from 0000 UTC 15 November 2018 to 0000 UTC 15 February 2019). The mean SLP distribution represents cyclone activity, and streamlines indicate flows near the surface. Around the Antarctic continent, there exist three minima in mean SLP, namely, over (1) the Weddell Sea and King Haakon XII Sea, (2) the Indian Ocean sector of the Southern Ocean off Wilkes Land, and (3) the Bellingshausen Sea and Amundsen Sea. This is consistent with Figure 4b in Wei and Qin (2016). We define three regions in the longitudinal direction, based on Figure 10a: R1 (the Weddell Sea and King Haakon XII Sea;

60° W–30° E), R2 (the Indian Ocean sector of the Southern Ocean; 90° E–150° E), and R3 (Bellingshausen Sea and Amundsen Sea; 150° W–60° W). Cyclonic circulation prevails around Antarctica, with some flow from the continent to the surrounding oceans.

Figure 11a shows the TEE of the CTL and YOPP experiments over three regions (i.e., R1, R2, and R3) as a function of forecast lead time. Regardless of the experiment, the TEE for the R2 region is the smallest, whereas that for the R3 region is the largest. This is because the R2 region is well observed by both routine and YOPP-SH SOP observations; in contrast, the number of observations over the R3 region is relatively small, even considering the extra

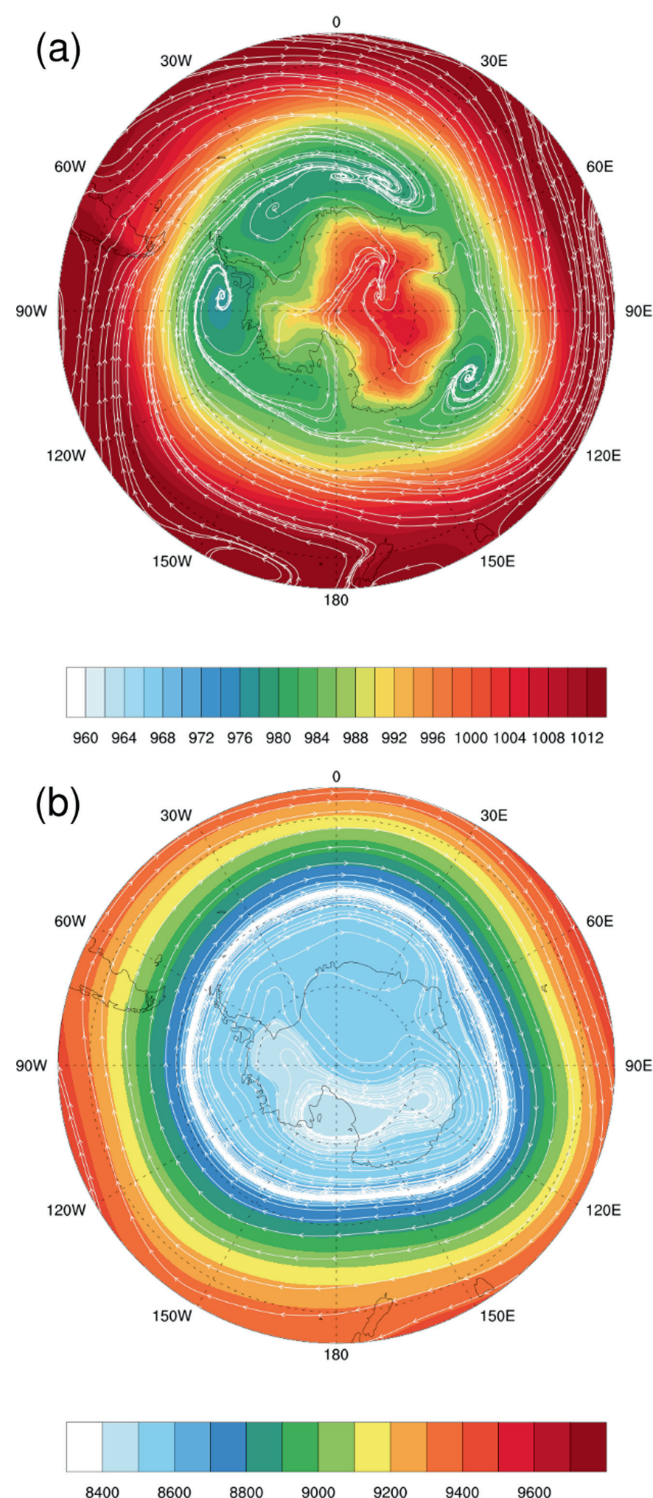


FIGURE 10 Horizontal distributions of (a) sea level pressure (SLP, shading, hPa) and 10-m streamline, and (b) geopotential height (shading, m) and streamline at 300 hPa. Six-hourly ERA5 re-analysis data are averaged from 0000 UTC 15 November 2018 to 0000 UTC 15 February 2019.

YOPP-SH observations (Figure 12a). Figure 11b–d show the differences in TEE between the CTL and YOPP experiments for the R1–R3 regions. Positive values indicate that TEE is reduced in YOPP compared to that in CTL. In R1, the difference in TEE at the analysis time (i.e., 0-hr lead time) is the largest compared to that in the other regions. The largest improvement of the analyses in the YOPP experiment is attributed to the increased number of radiosonde observations in R1 from the YOPP-SH SOP radiosonde launches (Figure 12a). In R1, the TEE difference decreases for approximately 24 hours, then increases for about 18 hours, and decreases again at 42-hr lead time. The increase of TEE at 24-hr lead time results from the spreading of the effects of assimilating additional observations from upstream regions by the prevailing cyclonic circulation around Antarctica. The difference in TEE at analysis time for R2 is the second-largest among all regions. The difference decreases slightly, until rising at a forecast lead time of 30 hours and then falling again at 42-hr lead time. A considerable increase in the TEE at 30-hr lead time is contributed by spreading the impact of assimilating the observations in the upstream regions. Finally, in R3, the difference in TEE at the analysis time is the smallest, owing to the small number of added observations from the YOPP-SH SOP launches (Figure 12a). After an initial decrease, the difference increases at 24-hr forecast lead time and then repeatedly increases and decreases. Although the absolute value of the difference at 42-hr lead time is not large, an increased difference between the 24-hr and 42-hr lead times is the greatest due to the spreading of assimilation effects from upstream regions where there were many YOPP-SH SOP soundings. To sum up, the difference in TEE at analysis time is the largest (smallest) in the R1 (R3) region, where the number of added radiosonde observations is the largest (smallest). In all regions, after an initial drop, the TEE difference increases at lead times of between 24 and 30 hours. This increase reflects the spreading of assimilation impact from the upstream regions; it is the largest in the R3 region because the R3 region is located downstream of East Antarctica, where there were a large number of YOPP-SH SOP radiosonde launches.

To check whether there is any impact spreading in the latitudinal direction, we define another three regions in the latitudinal direction: R4 (90° S–75° S), R5 (75° S–60° S), and R6 (60° S–45° S). Figure 13a shows the TEE of the CTL and YOPP experiments for regions R4–6. The TEE for R6 is the smallest at the analysis time, but becomes the largest beyond the forecast lead time of 96 hours. This may be because updated lateral boundary conditions initially constrain forecasts in R6; however, there are nearly no added observations to keep its forecasts accurate as the forecast length increases. Figure 13b–d shows the differences in TEE between the CTL and YOPP experiments for

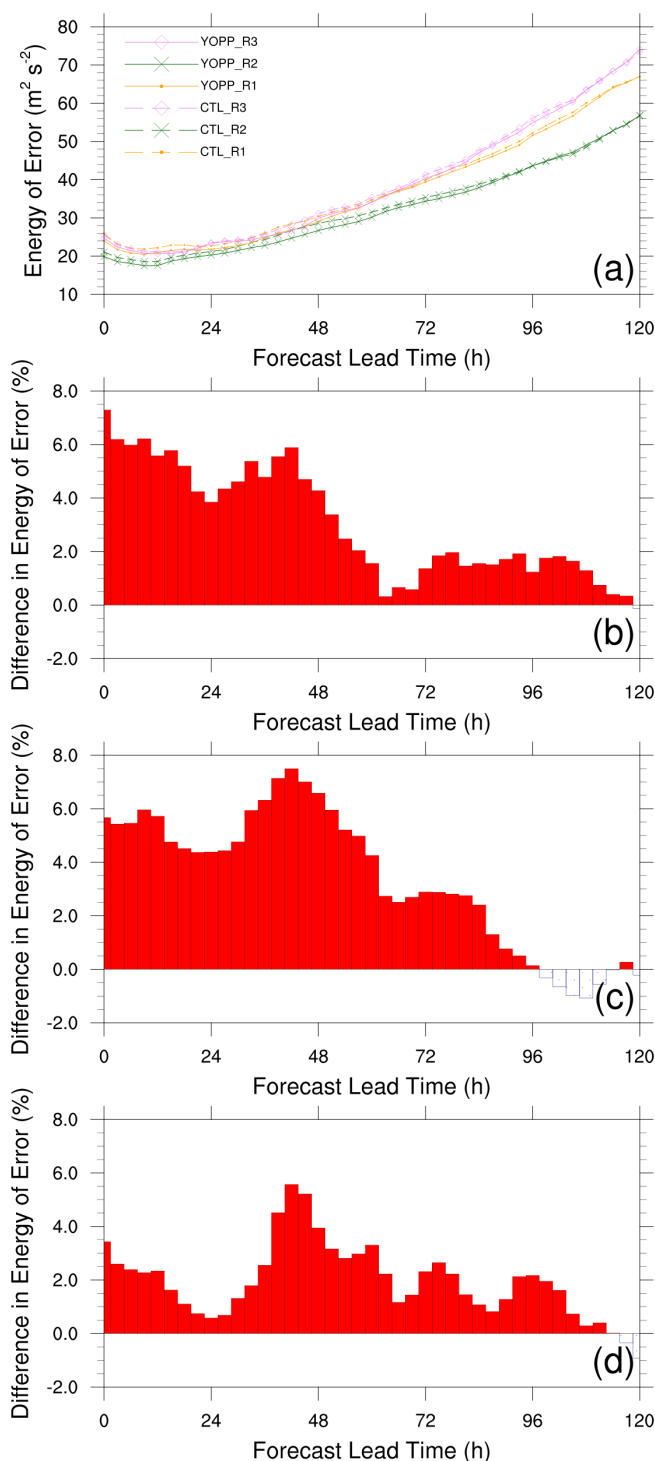


FIGURE 11 (a) Energy of error ($\text{m}^2 \text{s}^{-2}$) computed over Region 1 (orange dot), Region 2 (green cross), and Region 3 (pink diamond) for CTL (dashed line) and YOPP (solid line) experiments as a function of forecast lead time. Percentage difference (%) in error energy between CTL and YOPP experiments (CTL minus YOPP) for (b) Region 1, (c) Region 2, and (d) Region 3. Regions 1–3 are defined by longitude, R1: 60°W – 30°E , R2: 90°E – 150°E , and R3: 150°W – 60°W . [Colour figure can be viewed at [wileyonlinelibrary.com](https://onlinelibrary.wiley.com/doi/10.1002/qj.4528)]

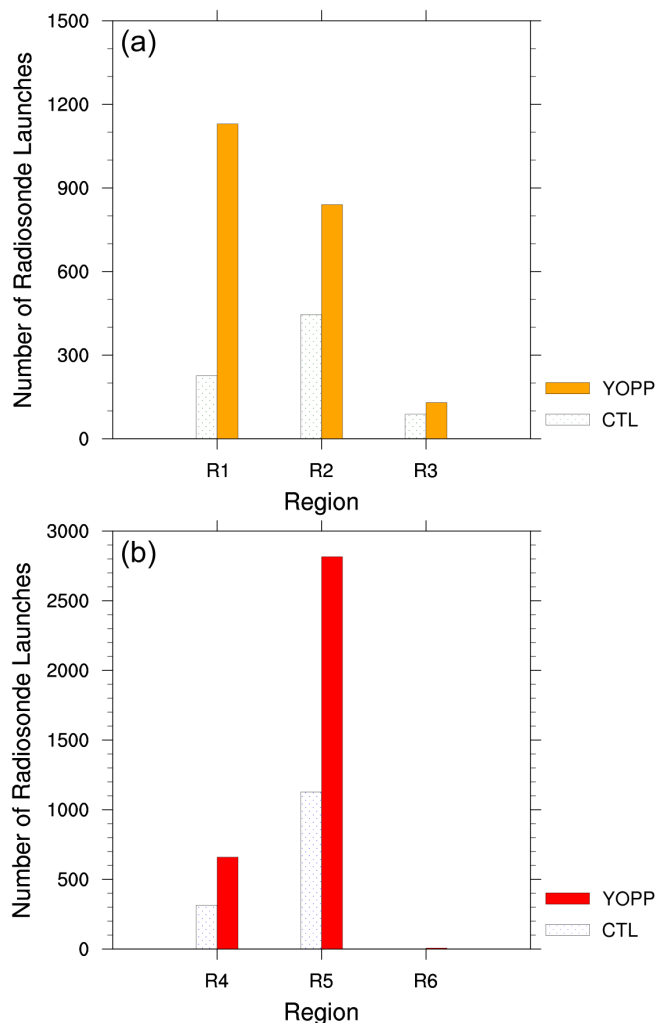


FIGURE 12 The number of radiosonde launches assimilated in CTL and YOPP experiments for (a) Regions 1–3 and (b) Regions 4–6. Regions 1–3 are defined by longitude (R1: 60°W – 30°E , R2: 90°E – 150°E , and R3: 150°W – 60°W), and Regions 4–6 are defined by latitude (R4: 90°S – 75°S , R5: 75°S – 60°S , and R6: 60°S – 45°S). [Colour figure can be viewed at [wileyonlinelibrary.com](https://onlinelibrary.wiley.com/doi/10.1002/qj.4528)]

the three regions. In R4, the difference in TEE at analysis time is the largest of the regions although the number of routine radiosonde observations is much smaller in R4 than in R5. This is because the number of assimilated observations in the YOPP experiment is more than double that in the CTL experiment (Figure 12b). In R4, the TEE difference decreases until 27-hr lead time and then becomes fluctuating. The increase between the 27- and 42-hr lead times is caused by the spreading of the effects of assimilating additional observations from lower latitudes (i.e., R5). Although there is no flow from the coastal to inland regions near the surface, at the 300-hPa level, streamlines show flows from the Weddell Sea and Ross Sea to the South Pole (Figure 10b). This impact spreading from coastal to inland regions is addressed further in the

next paragraph. The difference in TEE in the R5 region changes little, at least up to 72-hr forecast lead time. This is because a large number of additional observations along the coast are assimilated in the YOPP experiment. Through prevailing cyclonic circulation, the effects of the YOPP-SH observations persist to longer lead times. Finally, in R6, the difference in TEE is positive, despite almost no added observations. This is because the effects of assimilation in R5 spread into R6.

As seen in Equation (2), TEE is a vertically integrated value consisting of three kinds of energy: energy from wind, temperature, and moisture variables. Figure 14 shows the vertical distributions of the differences in the three kinds of error energy between the CTL and YOPP experiments as a function of the forecast lead time. A positive value indicates that the error energy is reduced in the YOPP experiment compared to that in the CTL experiment. At the analysis time (i.e., 0-hr lead time), temperature-related energy is dominant at lower levels, with a peak at the 925-hPa level. After 24 hours, energy from the winds emerges at the upper levels, although temperature-related energy at the lower levels is still prominent. At 48-hr lead time, wind-related energy at the upper levels (with a peak at the 300-hPa level) becomes dominant and remains so to 96 hours. In short, initially, the assimilation of YOPP-SH SOP observations affects the temperature at lower levels the most. Then, the assimilation effects spread into the winds at upper levels within 48 hours. These characteristics of the vertical propagation of the error energy are similar to those of singular vectors in mid-latitude regions (Ehrendorfer and Errico, 1995). This implies that, at high latitudes, mass fields can drive wind fields, as in the mid-latitudes. Bromwich *et al.* (2022) explained the improvement of lower-level temperature forecasts at earlier time and higher-level wind forecasts at later time in terms of the thermal wind. It should be noted that until the 96-hr lead time, the assimilation's impact on all three variables is positive at almost all pressure levels. This also explains the reason why the impact spreading from coastal to inland regions can occur after 24-hr lead time when error energy reduction at upper levels starts to grow.

4.4 | Case study

Forecasts from the cycle of 1200 UTC 19 December 2018 are chosen to look into how the assimilation of additional radiosonde observations from the YOPP-SH SOP positively affects subsequent forecasts. This case was selected because of cyclonic development over the Amundsen Sea, where a climatological low-pressure center is located (known as the Amundsen Sea Low), and

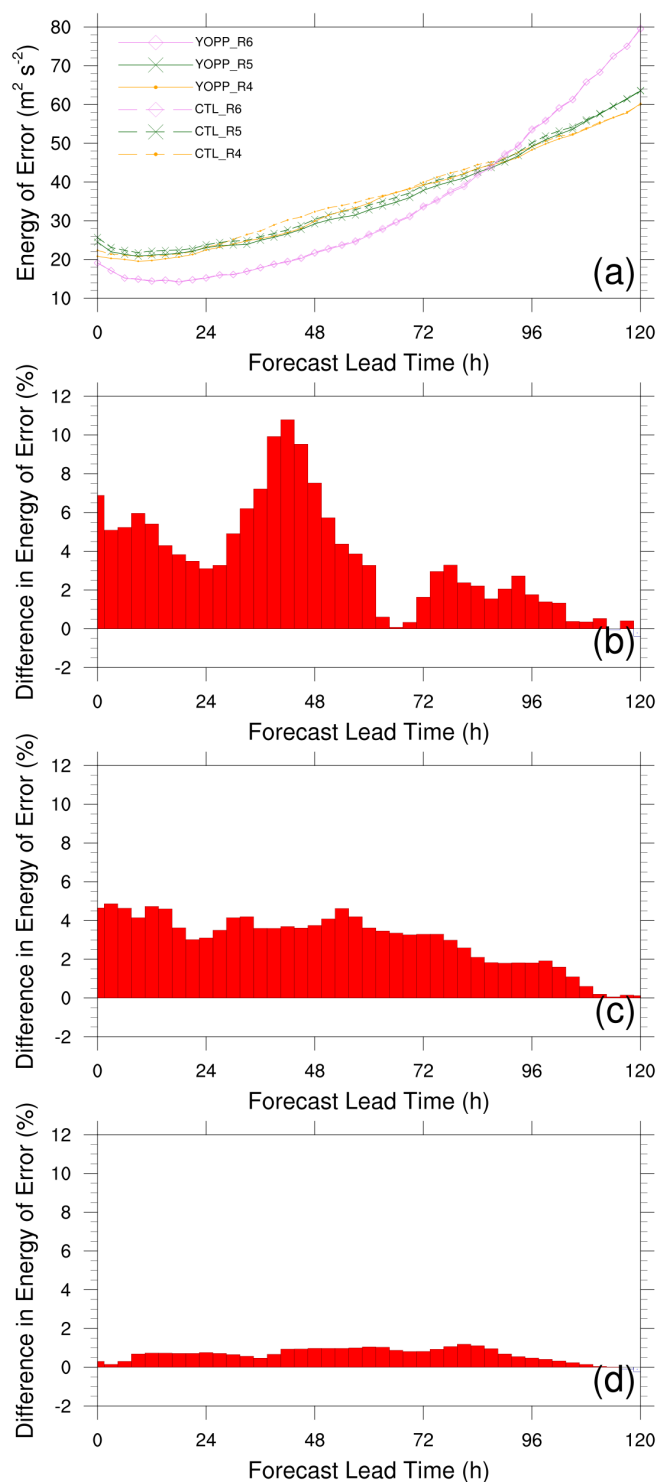


FIGURE 13 (a) Energy of error ($\text{m}^2 \text{s}^{-2}$) computed over Region 4 (orange dot), Region 5 (green cross), and Region 6 (pink diamond) for CTL (dashed line) and YOPP (solid line) experiments as a function of forecast lead time. Percentage difference (%) in error energy between CTL and YOPP experiments (CTL minus YOPP) for (b) Region 4, (c) Region 5, and (d) Region 6. Regions 4–6 are defined by latitude, R4: 90–75° S, R5: 75° S–60° S, and R6: 60° S–45° S. [Colour figure can be viewed at wileyonlinelibrary.com]

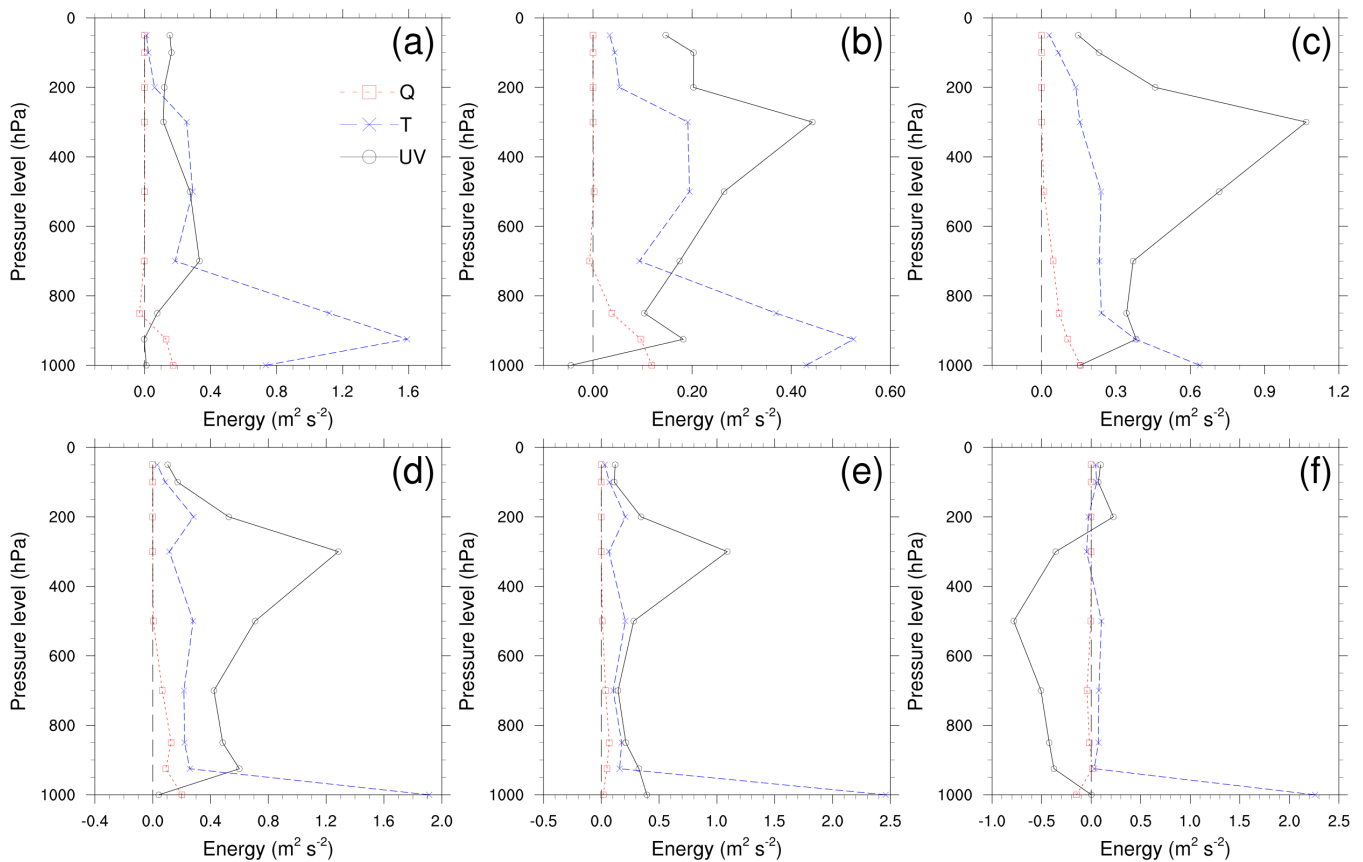


FIGURE 14 Vertical distributions of difference in error energy ($\text{m}^2 \text{s}^{-2}$) between CTL and YOPP experiments (CTL minus YOPP) at lead times of (a) 0, (b) 24, (c) 48, (d) 72, (e) 96, and (f) 120 hours. Energy related to wind (black solid line with circle), temperature (blue dashed line with cross), and moisture (red dotted line with square) is shown. [Colour figure can be viewed at [wileyonlinelibrary.com](https://onlinelibrary.wiley.com/doi/10.1002/qj.4528)] See the Terms and Conditions (<https://onlinelibrary.wiley.com/terms-and-conditions>) on Wiley Online Library for rules of use; OA articles are governed by the applicable Creative Commons License

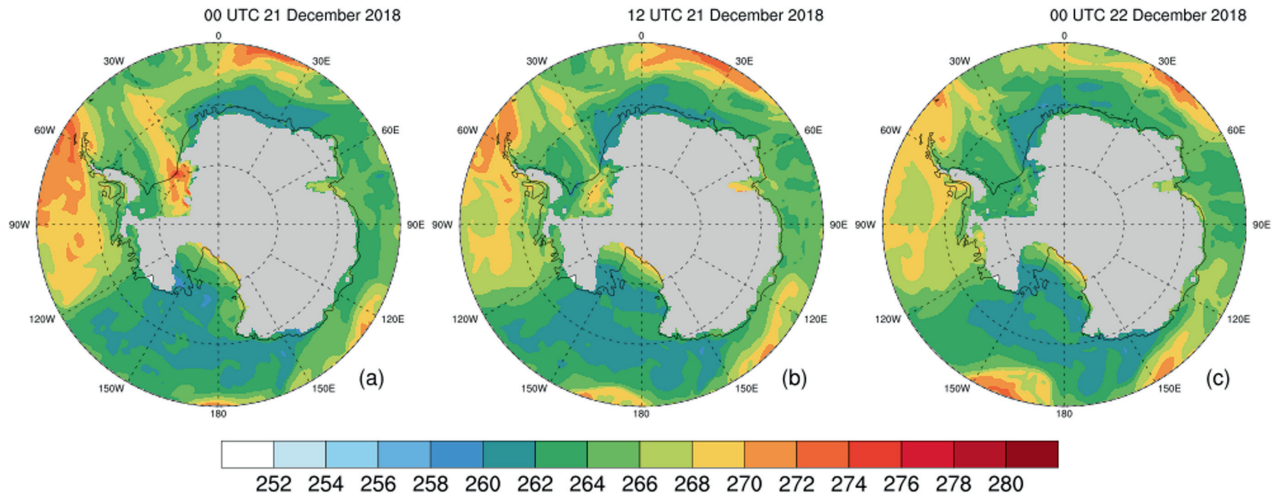
the Amundsen Sea Low significantly impacts West Antarctic climate, including temperature, sea-ice extent, and precipitation (Goyal *et al.*, 2021). Figure 15 shows the horizontal distributions of the 850-hPa temperature from the ERA5 re-analysis, the 850-hPa temperature error in CTL, and difference in the 850-hPa temperature between CTL and YOPP (YOPP minus CTL), for the period of 0000 UTC 21 December to 0000 UTC 22 December 2018. The horizontal temperature gradient was maintained between warm air east of 120°W and cool air west of 120°W in the ERA5 re-analysis (Figure 15a–c). In the forecasts of the CTL experiment, there are cold biases over the Amundsen Sea and warm biases over the Ross Ice Shelf; these biases lead to a reduced horizontal temperature gradient over the region of interest (Figure 15d–f). Through assimilation of YOPP-SH SOP radiosonde observations, the cold and warm biases are dramatically diminished in the YOPP experiment (Figure 15g–i). The horizontal distributions of the 850-hPa geopotential height from the ERA5 re-analysis, its error in the CTL experiment, and its difference between the CTL and YOPP experiments (YOPP minus CTL) are

shown in Figure 16. The cyclone over the Bellingshausen and Amundsen Seas deepened from 0000 UTC to 1200 UTC 21 December 2018 and then weakened for the next 12 hours in the ERA5 re-analysis (Figure 16a–c). In the CTL experiment, the cyclone is weaker than in the re-analysis owing to decreased baroclinicity, and negative height biases appear over Ross Ice Shelf (Figure 16d–f). Improved forecasts of 850-hPa temperature in YOPP are evidenced by a more accurate intensity of the forecast cyclone and smaller height biases over Ross Ice Shelf (Figure 16g–i).

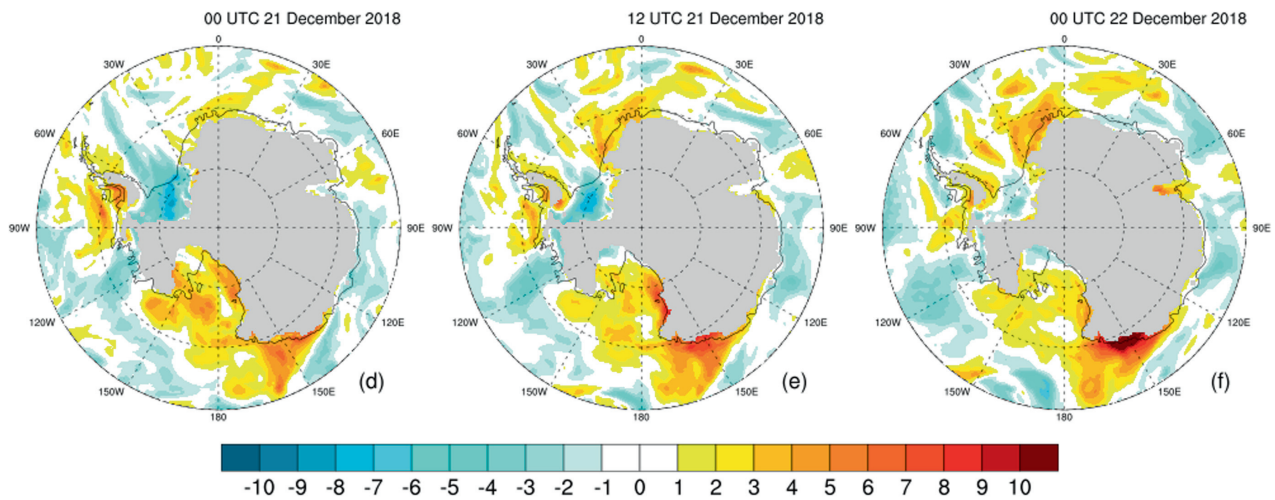
5 | SUMMARY AND CONCLUSIONS

The effects of assimilating additional radiosonde observations from the YOPP-SH SOP were investigated by conducting OSEs. In the CTL experiment, routine radiosonde observations together with the other conventional, GPS RO, and radiance observations were assimilated; in the YOPP experiment, extra observations from enhanced radiosonde launches were additionally

ERA5 reanalysis (850-hPa T)



Error of CTL (850-hPa T)



Difference between CTL and YOPP (850-hPa T)

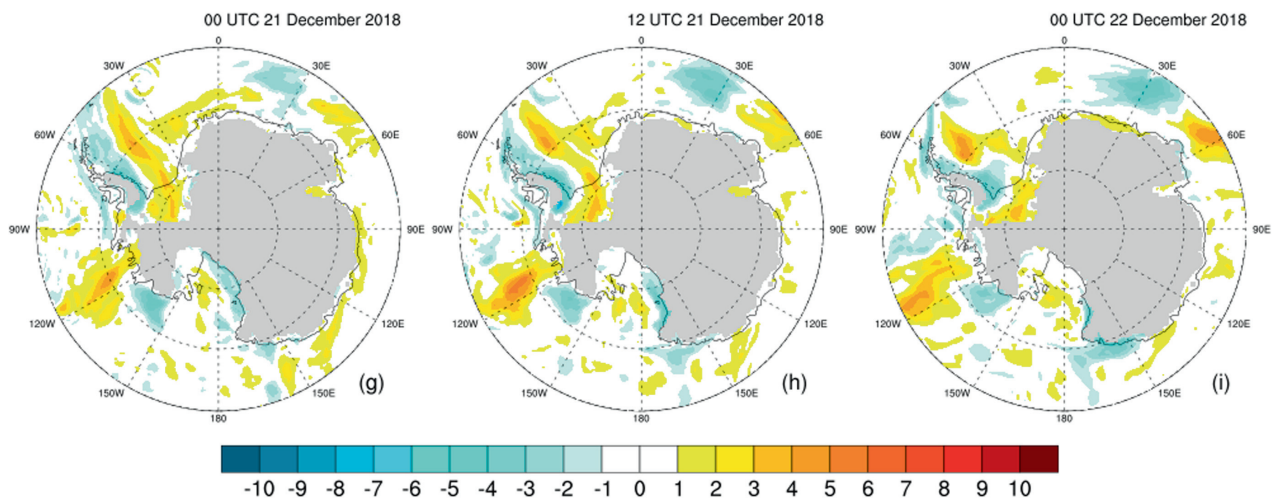
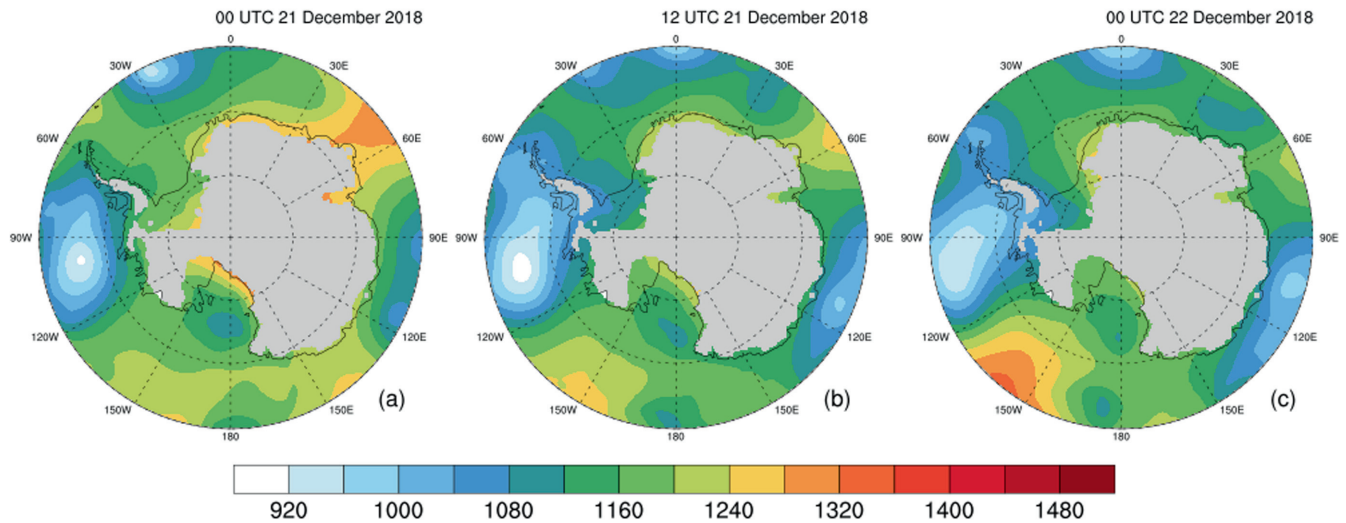
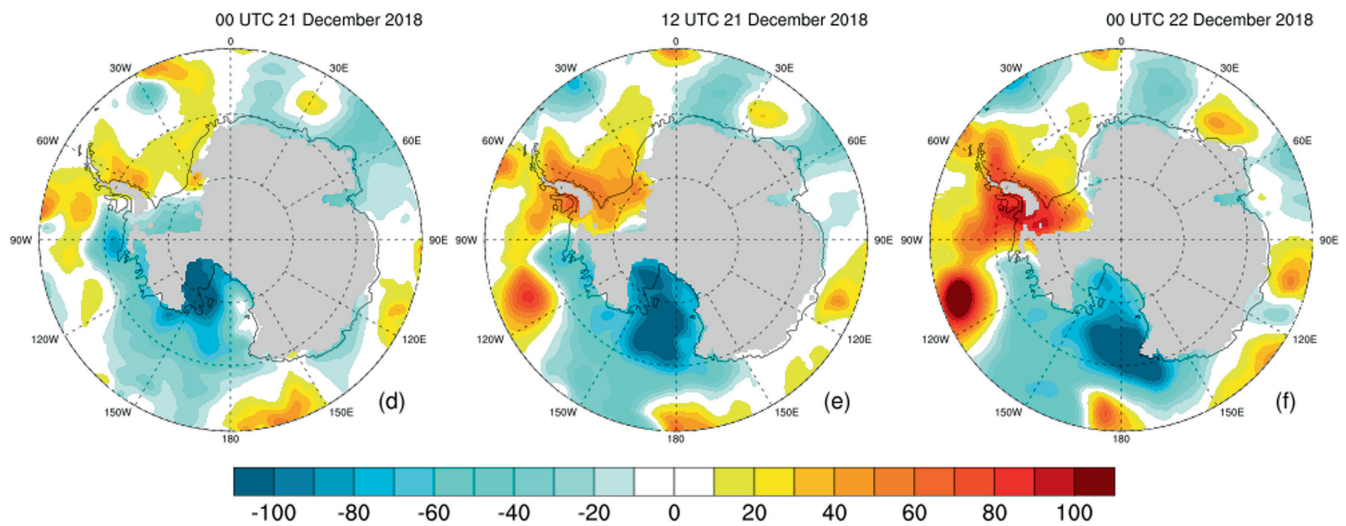


FIGURE 15 Horizontal distributions of (a–c) 850-hPa temperature (K) from ERA5 re-analysis, (d–f) its error (K) in CTL experiment, and (g–i) its difference (K) between CTL and YOPP experiments (YOPP minus CTL) from 0000 UTC 21 to 0000 UTC 22 December 2018, with an interval of 12 hours. Forecasts initialized at 1200 UTC 19 December 2018 are used. Areas where 850-hPa surface is below the ice sheet are gray-shaded.

ERA5 reanalysis (850-hPa Z)



Error of CTL (850-hPa Z)



Difference between CTL and YOPP (850-hPa Z)

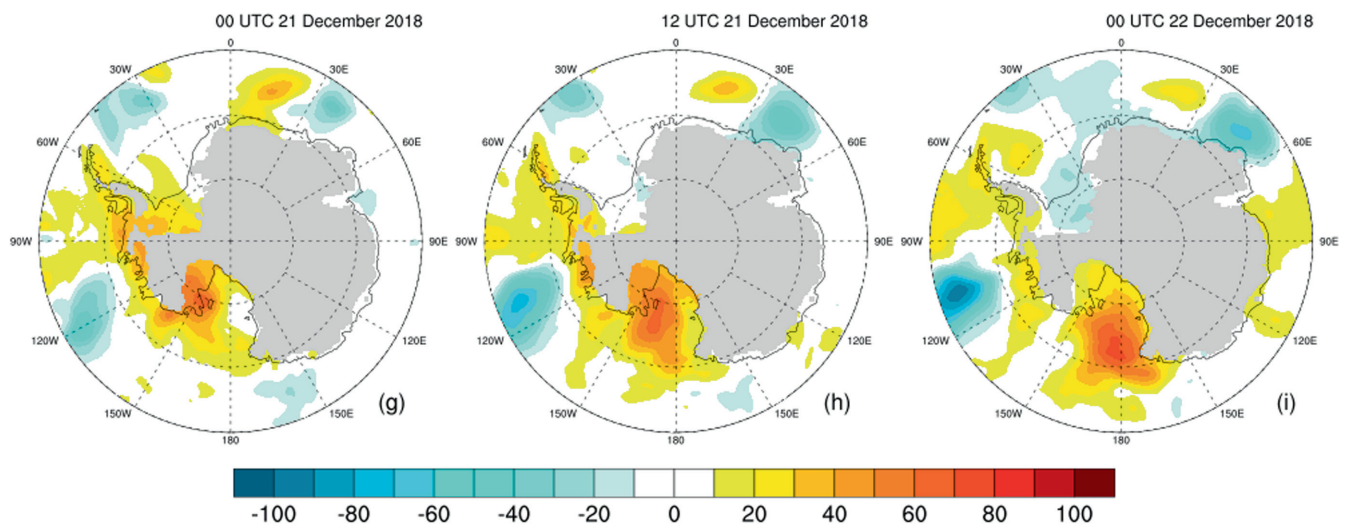


FIGURE 16 Same as Figure 15 except for 850-hPa geopotential height (m).

assimilated. Verification of analyses and forecasts from the two experiments was conducted against ERA5 re-analysis, radiosonde observations, and AWS observations, and the results were compared to reveal the effects of the extra radiosonde data on analyses and forecasts over Antarctica. A case study was done to identify the reason for the forecast improvement in the YOPP experiment, which was shown in the verification statistics for the DA cycling period. Furthermore, how the DA effects spread in the longitudinal, latitudinal, and vertical directions was examined.

The results of this study can be summarized as follows:

1. Verification against ERA5 re-analysis, radiosonde observations, and AWS observations shows that both analyses and forecasts are improved by assimilating additional radiosonde observations from YOPP-SH SOP.
2. Effects of additional radiosonde observations are larger for south of 60° S than north of 60° S and they are greater for a period of January 1–17, 2019 than for the whole SOP.
3. The forecast improvement of temperature and moisture variables manifests at lower levels, whereas that of wind variables appears at the upper levels.
4. DA effects spread in both the longitudinal and latitudinal directions; this spreading can offset the deficiencies in model forecasts that may attend observational data gaps in western and inland Antarctica.
5. Initially, the effects of additional radiosonde observations are noticeable in temperature in the lower troposphere, but at later forecast hours the improvements are seen in the winds at the upper-tropospheric levels.
6. The results of this study (e.g., spreading of DA effect) provide insights into future observation strategies over Antarctica.
7. Some of the conclusions of this study (i.e., #1, 2, 3, and 5) are consistent with the previous study of Bromwich *et al.* (2022).
8. This study uniquely analyzed spreading of DA effects using the TEE metric. The DA effects spread in the longitudinal direction through a cyclonic circulation surrounding Antarctica, and they also spread in the latitudinal direction. The spread of DA effects helps to improve forecasts in western and inland Antarctica, where the number of radiosonde observations is less.

The quantitative impact of additional radiosonde observations can be measured by the dRMSE metric. When considering effects on the whole domain and cycling period, maximum dRMSEs for wind, temperature, and geopotential height variables are in the range of 1.97%–3.87%. Maximum dRMSEs have increased values in

the range of 2.34%–4.47%, 2.86%–4.53%, and 3.60%–5.45% when the smaller areas (i.e., south of 60° S where most additional radiosonde observations are located), shorter period (i.e., January 1–17, 2019 when the number of additional radiosonde observations is greatest), and both of them are considered. These numbers are comparable to the results of previous studies that showed effects of radiosonde observations over polar regions (e.g., Boulot *et al.*, 2016; Lawrence *et al.*, 2019). As the number of conventional observations is relatively few, and the use of radiance observations is limited over Antarctica, it is important scientifically and economically to understand the enhancement of atmospheric observation over Antarctica based on the evaluation of added measurements (e.g., by performing observing system simulation experiments).

The effects of additional radiosonde observations can be maximized by adopting a more sophisticated DA method (e.g., hybrid, 4D-Var) and also by considering balloon drift. In 2022, the YOPP-SH program winter Targeted Observing Period (TOP) was conducted and extra radiosondes were again launched. This will provide another opportunity for investigations of how to best exploit the special radiosonde observations.

AUTHOR CONTRIBUTIONS

Yonghan Choi: Conceptualization; formal analysis; investigation; methodology; software; validation; visualization; writing – original draft; writing – review and editing. **Seong-Joong Kim:** Funding acquisition; investigation; project administration; writing – review and editing. **David H. Bromwich:** Investigation; writing – review and editing. **Jordan Powers:** Investigation; writing – review and editing. **Hataek Kwon:** Investigation; writing – review and editing. **Sang-Jong Park:** Conceptualization; data curation; investigation; methodology; supervision; writing – review and editing.


ACKNOWLEDGEMENTS

Yonghan Choi, Seong-Joong Kim, and Sang-Jong Park were supported by the Korea Polar Research Institute (KOPRI) grant funded by the Ministry of Oceans and Fisheries (KOPRI PE23030). David H. Bromwich and Jordan G. Powers were supported by NSF grant 2205398. This work is a contribution to the Year of Polar Prediction (YOPP), a flagship activity of the Polar Prediction Project (PPP), initiated by the World Weather Research Program (WWRP) of the World Meteorological Organization (WMO). Contribution C-1623 of Byrd Polar and Climate Research Center. Hataek Kwon was supported by the National Research Foundation of Korea (NRF) grant funded by the Korea government (NRF-2023R1A2C1008238). Authors are grateful

to the editor and anonymous reviewers for their valuable comment.

ORCID

Yonghan Choi  <https://orcid.org/0000-0002-6617-4850>

Seong-Joong Kim  <https://orcid.org/0000-0002-6232-8082>

David H. Bromwich  <https://orcid.org/0000-0003-4608-8071>

Sang-Jong Park  <https://orcid.org/0000-0002-6944-6962>

REFERENCES

- Barker, D., Huang, X.-Y., Liu, Z., Auligné, T., Zhang, X., Rugg, S., Ajjaji, R., Al Bourgeois, J.B., Chen, Y., Demirtas, M., Guo, Y.-R., Henderson, T., Huang, W., Lin, H.-C., Michalakes, J., Rizvi, S. and Zhang, X. (2012) The weather research and forecasting model's community variational/ensemble data assimilation system: WRFDA. *Bulletin of the American Meteorological Society*, 93, 831–843.
- Boullot, N., Rabier, F., Langland, R., Gelaro, R., Cardinali, C., Guidard, V., Bauer, P. and Doerenbecher, A. (2016) Observation impact over the southern polar area during the Concordiasi field campaign. *Quarterly Journal of the Royal Meteorological Society*, 142, 597–610.
- Bromwich, D.H., Powers, J.G., Manning, K.W. and Zou, X. (2022) Antarctic data impact experiments with polar WRF during the YOPP-SH summer special observing period. *Quarterly Journal of the Royal Meteorological Society*, 148, 2194–2218.
- Bromwich, D.H., Werner, K., Casati, B., Powers, J.G., Gorodetskaya, I.V., Massonnet, F., Vitale, V., Heinrich, V.J., Liggett, D., Arndt, S., Barja, B., Bazile, E., Carpentier, S., Carrasco, J.F., Choi, T., Choi, Y., Colwell, S.R., Cordero, R.R., Gervasi, M., Haiden, T., Hirasawa, N., Inoue, J., Jung, T., Kalesse, H., Kim, S.-J., Lazzara, M.A., Manning, K.W., Norris, K., Park, S.-J., Reid, P., Rigor, I., Rowe, P.M., Schmithüsen, H., Seifert, P., Sun, Q., Uttal, T., Zannoni, M. and Zou, X. (2020) The year of polar prediction in the southern hemisphere (YOPP-SH). *Bulletin of the American Meteorological Society*, 101, E1653–E1676.
- Cohen, J., Agel, L., Barlow, M., Garfinkel, C.I. and White, I. (2021) Linking Arctic variability and change with extreme winter weather in the United States. *Science*, 373, 1116–1121.
- Dee, D.P. (2004) Variational Bias Correction of Radiance Data in the ECMWF System. Reading, UK: Proceedings of the ECMWF workshop on assimilation of high spectral resolution sounders in NWP, pp. 97–112.
- Dong, X., Wang, Y., Hou, S., Ding, M., Yin, B. and Zhang, Y. (2020) Robustness of the recent global atmospheric reanalyses for Antarctic near-surface wind speed climatology. *Journal of Climate*, 33, 4027–4043.
- Ehrendorfer, M. and Errico, R.M. (1995) Mesoscale predictability and the spectrum of optimal perturbations. *Journal of Atmospheric Sciences*, 52, 3475–3500.
- Ehrendorfer, M., Errico, R.M. and Raeder, K.D. (1999) Singular-vector perturbation growth in a primitive equation model with moist physics. *Journal of the Atmospheric Sciences*, 56, 1627–1648.
- Gossart, A., Helsen, S., Lenaerts, J., Broucke, S.V., Van Lipzig, N. and Souverijns, N. (2019) An evaluation of surface climatology in state-of-the-art reanalyses over the Antarctic ice sheet. *Journal of Climate*, 32, 6899–6915.
- Goyal, R., Jucker, M., Gupta, A.S. and England, M.H. (2021) Generation of the Amundsen Sea low by Antarctic orography. *Geophysical Research Letters*, 48, e2020GL091487.
- Graham, R.M., Cohen, L., Ritzhaupt, N., Segger, B., Graversen, R.G., Rinke, A., Walden, V.P., Granskog, M.A. and Hudson, S.R. (2019a) Evaluation of six atmospheric reanalyses over Arctic Sea ice from winter to early summer. *Journal of Climate*, 32, 4121–4143.
- Graham, R.M., Hudson, S.R. and Maturilli, M. (2019b) Improved performance of ERA5 in Arctic gateway relative to four global atmospheric reanalyses. *Geophysical Research Letters*, 46, 6138–6147.
- Grell, G.A. and Freitas, S.R. (2014) A scale and aerosol aware stochastic convective parameterization for weather and air quality modeling. *Atmospheric Chemistry and Physics*, 14, 5233–5250.
- Gu, M., Wang, Z., Wei, J. and Yu, X. (2021) An assessment of Arctic cloud water paths in atmospheric reanalyses. *Acta Oceanologica Sinica*, 40, 46–57.
- Han, Y., van Delst, P., Liu, Q., Weng, F., Yan, B., Treadon, R. and Derber, J. (2006) *JCSDA Community Radiative Transfer Model (CRTM): Version 1*. NOAA, Washington, D. C.: NOAA Technical Report.
- Harrison, T.C., Biri, S., Bracegirdle, T.J., King, J.C., Kent, E.C., Vignon, É. and Turner, J. (2022) Reanalysis representation of low-level winds in the Antarctic near-coastal region. *Weather and Climate Dynamics*, 3, 1415–1437.
- Hong, S.-Y., Dudhia, J. and Chen, S.-H. (2004) A revised approach to ice microphysical processes for the bulk parameterization of clouds and precipitation. *Monthly Weather Review*, 132, 103–120.
- Iacono, M.J., Delamere, J.S., Mlawer, E.J., Shephard, M.W., Clough, S.A. and Collins, W.D. (2008) Radiative forcing by long-lived greenhouse gases: calculations with the AER radiative transfer models. *Journal of Geophysical Research: Atmospheres*, 113, D13103.
- Inoue, J., Enomoto, T. and Hori, M.E. (2013) The impact of radiosonde data over the ice-free Arctic Ocean on the atmospheric circulation in the northern hemisphere. *Geophysical Research Letters*, 40, 864–869.
- Inoue, J., Yamazaki, A., Ono, J., Dethloff, K., Maturilli, M., Neuber, R., Edwards, P. and Yamaguchi, H. (2015) Additional Arctic observations improve weather and sea-ice forecasts for the Northern Sea route. *Scientific Reports*, 5, 1–8.
- Janjić, Z.I. (1994) The step-mountain eta coordinate model: further developments of the convection, viscous sublayer, and turbulence closure schemes. *Monthly Weather Review*, 122, 927–945.
- Jun, S.-Y., Kim, J.-H., Choi, J., Kim, S.-J., Kim, B.-M. and An, S.-I. (2020) The internal origin of the west-east asymmetry of Antarctic climate change. *Science Advances*, 6, eaaz1490.
- Lawrence, H., Bormann, N., Sandu, I., Day, J., Farnan, J. and Bauer, P. (2019) Use and impact of Arctic observations in the ECMWF numerical weather prediction system. *Quarterly Journal of the Royal Meteorological Society*, 145, 3432–3454.
- Lee, M.-H., Kim, J.-H., Song, H.-J., Inoue, J., Sato, K. and Yamazaki, A. (2019) Potential benefit of extra radiosonde observations around the Chukchi Sea for the Alaskan short-range weather forecast. *Polar Science*, 21, 124–135.
- Liu, Z., Schwartz, C.S., Snyder, C. and Ha, S.-Y. (2012) Impact of assimilating AMSU-A radiances on forecasts of 2008 Atlantic tropical cyclones initialized with a limited-area ensemble Kalman filter. *Monthly Weather Review*, 140, 4017–4034.

- Naakka, T., Nygård, T., Tjernström, M., Vihma, T., Pirazzini, R. and Brooks, I.M. (2019) The impact of radiosounding observations on numerical weather prediction analyses in the Arctic. *Geophysical Research Letters*, 46, 8527–8535.
- Ono, J., Inoue, J., Yamazaki, A., Dethloff, K. and Yamaguchi, H. (2016) The impact of radiosonde data on forecasting sea-ice distribution along the Northern Sea route during an extremely developed cyclone. *Journal of Advances in Modeling Earth Systems*, 8, 292–303.
- Parrish, D.F. and Derber, J.C. (1992) The National Meteorological Center's spectral statistical-interpolation analysis system. *Monthly Weather Review*, 120, 1747–1763.
- Randriamampianina, R., Bormann, N., Koltzow, M.A.Ø., Lawrence, H., Sandu, I. and Wang, Z.Q. (2021) Relative impact of observations on a regional Arctic numerical weather prediction system. *Quarterly Journal of the Royal Meteorological Society*, 147, 2212–2232.
- Sato, K., Inoue, J., Alexander, S.P., McFarquhar, G. and Yamazaki, A. (2018a) Improved reanalysis and prediction of atmospheric fields over the Southern Ocean using campaign-based radiosonde observations. *Geophysical Research Letters*, 45, 11406–11413.
- Sato, K., Inoue, J., Yamazaki, A., Hirasawa, N., Sugiura, K. and Yamada, K. (2020) Antarctic radiosonde observations reduce uncertainties and errors in reanalyses and forecasts over the Southern Ocean: An extreme cyclone case. *Advances in Atmospheric Sciences*, 37, 431–440.
- Sato, K., Inoue, J., Yamazaki, A., Tomikawa, Y. and Sato, K. (2022) Reduced error and uncertainty in analysis and forecasting in the southern hemisphere through assimilation of PANSY radar observations from Syowa station: a midlatitude extreme cyclone case. *Quarterly Journal of the Royal Meteorological Society*, 148, 3115–3130.
- Sato, K., Inoue, J., Yamazaki, A., Kim, J.-H., Makshtas, A., Kustov, V., Maturilli, M. and Dethloff, K. (2018b) Impact on predictability of tropical and mid-latitude cyclones by extra Arctic observations. *Scientific Reports*, 8, 1–8.
- Sato, K., Inoue, J., Yamazaki, A., Kim, J.-H., Maturilli, M., Dethloff, K., Hudson, S.R. and Granskog, M.A. (2017) Improved forecasts of winter weather extremes over midlatitudes with extra Arctic observations. *Journal of Geophysical Research: Oceans*, 122, 775–787.
- Skamarock, W.C., Klemp, J.B., Dudhia, J., Gill, D.O., Liu, Z., Berner, J., Wang, W., Powers, J.G., Duda, M.G., Barker, D.M. and Huang, X.-Y. (2019) A description of the advanced research WRF version 4. *NCAR tech. Note NCAR/TN-556+STR*, 145.
- Soldatenko, S., Tingwell, C., Steinle, P. and Kelly-Gerreyn, B.A. (2018) Assessing the impact of surface and upper-air observations on the forecast skill of the ACCESS numerical weather prediction model over Australia. *Atmosphere*, 9, 23.
- Sun, Q., Vihma, T., Jonassen, M.O. and Zhang, Z. (2020) Impact of assimilation of radiosonde and UAV observations from the Southern Ocean in the polar WRF model. *Advances in Atmospheric Sciences*, 37, 441–454.
- Tetzner, D., Thomas, E. and Allen, C. (2019) A validation of ERA5 reanalysis data in the southern Antarctic peninsula—Ellsworth land region, and its implications for ice core studies. *Geosciences*, 9, 289.
- Tewari, M. (2004) Implementation and Verification of the Unified NOAA Land Surface Model in the WRF Model. Paper presented at: 20th conference on weather analysis and forecasting/16th conference on numerical weather prediction, pp. 2165–2170.
- Wang, C., Graham, R.M., Wang, K., Gerland, S. and Granskog, M.A. (2019) Comparison of ERA5 and ERA-interim near-surface air temperature, snowfall and precipitation over Arctic Sea ice: effects on sea ice thermodynamics and evolution. *The Cryosphere*, 13, 1661–1679.
- Wei, L. and Qin, T. (2016) Characteristics of cyclone climatology and variability in the Southern Ocean. *Acta Oceanologica Sinica*, 35, 59–67.
- Xin, M., Li, X., Zhu, J., Song, C., Zhou, Y., Wang, W. and Hou, Y. (2023) Characteristic features of the Antarctic surface air temperature with different reanalyses and in situ observations and their uncertainties. *Atmosphere*, 14, 464.
- Yamazaki, A., Inoue, J., Dethloff, K., Maturilli, M. and König-Langlo, G. (2015) Impact of radiosonde observations on forecasting summertime Arctic cyclone formation. *Journal of Geophysical Research: Atmospheres*, 120, 3249–3273.
- Yu, Y., Xiao, W., Zhang, Z., Cheng, X., Hui, F. and Zhao, J. (2021) Evaluation of 2-m air temperature and surface temperature from ERA5 and ERA-I using buoy observations in the arctic during 2010–2020. *Remote Sensing*, 13, 2813.
- Zhang, F., Snyder, C. and Rotunno, R. (2003) Effects of moist convection on mesoscale predictability. *Journal of the Atmospheric Sciences*, 60, 1173–1185.
- Zhu, J., Xie, A., Qin, X., Wang, Y., Xu, B. and Wang, Y. (2021) An assessment of ERA5 reanalysis for Antarctic near-surface air temperature. *Atmosphere*, 12, 217.

SUPPORTING INFORMATION

Additional supporting information can be found online in the Supporting Information section at the end of this article.

How to cite this article: Choi, Y., Kim, S.-J., Bromwich, D.H., Powers, J.G., Kwon, H. & Park, S.-J. (2023) Effects of assimilation of YOPP-SH additional radiosonde observations on analyses and forecasts over Antarctica in austral summer. *Quarterly Journal of the Royal Meteorological Society*, 149(756), 2719–2741. Available from: <https://doi.org/10.1002/qj.4528>